12-2011

Surface Wetting and Friction Studies of Nano-Engineered Surfaces on Copper Substrate

Julius Sheldon Morehead
University of Arkansas, Fayetteville

SURFACE WETTING AND FRICTION STUDIES OF NANO-ENGINEERED SURFACES ON COPPER SUBSTRATE

SURFACE WETTING AND FRICTION STUDIES OF NANO-ENGINEERED SURFACES ON COPPER SUBSTRATE

A thesis submitted in partial fulfillment
of the requirement for the degree of
Master of Science in Mechanical Engineering

By

Julius Morehead
University of Arkansas
Bachelor of Science in Mechanical Engineering, 2009

December 2011
University of Arkansas

ABSTRACT

Nano-engineered-textures on a material surface can dramatically improve the wetting and non-wetting properties of a surface, and they also show promise to address friction issues that affect surfaces in contact. In this work, aluminum-induced crystallization (AIC) of amorphous silicon (a-Si) was used to produce nano-textures on copper (Cu) substrates. A study was performed to examine the effects of changing the annealing conditions and a-Si thickness on nano-texture formation. The creation of various nano-topographies and chemically modifying them using octafluorocyclobutane (C_4F_8) was performed to control hydrophilicity, hydrophobicity, and oil affinity of nano-textured surfaces. A video-based contact angle measurement system was used to measure the surface wetting properties. Scanning electron microscopy (SEM) was employed to characterize the surface nano-topographies and provide a basis for qualitative and quantitative analysis of the nano-texture formations. Scratch testing was performed using a TriboIndenter to assess the potential of the nano-textured Cu substrates to lower the coefficient of friction (COF). It was found that the thicker a-Si layer generated larger textures overall which contributed to water contact angle (CA) results ranging between superhydrophilic and superhydrophobic, as well as increased oil affinity of Cu substrate. The nano-textured surfaces also achieved COF values that were 40 % lower than as-received (AR) Cu.

Key words: nano-surface engineering, AIC of a-Si, a-Si thickness effect, nano-textured Cu surfaces, COF analysis on Cu substrate.

This thesis is approved for recommendation
to the Graduate Council.

Thesis Director:

_____

Dr. Min Zou

Thesis Committee:

_____

Dr. Rick Couvillion

_____

Dr. Uchechukwu Wejinya

THESIS DUPLICATION RELEASE

I hereby authorize the University of Arkansas Libraries to duplicate this thesis when needed for research and/or scholarship.

Agreed _____

Julius Morehead

Refused _____

Julius Morehead

ACKNOWLEDGMENTS

Thank you to Dr. Min Zou, my advisor and director of the thesis committee, for your support throughout the course of this research. I also express appreciation to the members of the thesis committee: Dr. Rick Couvillion and Dr. Uchechukwu Wejinya. Special thanks to my colleague, Hengyu Wang, at the University of Arkansas for your help and guidance.

I wish also to thank the US National Science Foundation (NSF) for its support under grants CMS-0600642 and CMS-0645040, Dr. Andrew Wang from Ocean NanoTech, LLC, and the Electron Optics Facility (EOF) of the University of Arkansas for equipment use.

DEDICATION

This thesis is dedicated to my family for their love and support throughout my studies.

TABLE OF CONTENTS

LIST OF TABLES

LIST OF FIGURES

CHAPTER 1

INTRODUCTION

1.1 Background

As the size of engineered devices has been reduced to the microscale and smaller, the friction and adhesion caused by surface forces acting on these structures have proven to be detrimental to their operation [1]. Indeed, much effort has gone into the discovery of methods and new materials to deal effectively with problems encountered in the production of micro-electromechanical systems (MEMS) devices. The reliability issues associated with MEMS-based microstructures and the development of nano-electromechanical systems (NEMS) were partly responsible for the research that led to nano-surface engineering [1, 2]. Another important inspiration for the interest in nano-surface engineering was nature itself. Humans have always looked to nature for solutions to common engineering problems. For instance, nano-surface engineering played a significant role in the creation of nanoscale bio-mimetic surfaces that are useful in a variety of applications [3-5].

Nano-surface engineering to simultaneously affect a material's wetting and frictional behavior are fairly new areas of research. To introduce the research associated with these important topics, size-dependent properties at the nanoscale, surface wetting properties, and surface nano-texturing methods will be discussed. Presented, too, are the motivations for the research carried out in the preparation of this thesis and a description of the thesis organization.

1.1.1 Size-Dependent Properties at the Nanoscale

Matter on the nanoscale is known to possess physical, chemical, and biological properties which are different from the ones on the macro, molecular, and atomic scales [6]. The ability of materials to exhibit size-dependent behavior provides opportunity for them to become the focus of development as the next class of advanced materials [7]. On the nanoscale, a material's properties such as melting temperature, optical, magnetic, and electronic properties can be engineered to produce a change in its physical characteristics while maintaining the material's chemical composition or bulk properties [8]. For example, the optical and electrical properties of some nano-structures makes them suitable prospects for biological, photovoltaic, and chemical sensing uses [9-11]. Also, nanoscale textures on surfaces can change the surface's roughness and, consequently, the wetting property of the surfaces.

1.1.2 Surface Wetting Properties

Surface roughness can affect the wetting property of a surface, according to the Cassie-Baxter and Wenzel models which predict the wetting behavior of a surface based on roughness factor (Wenzel's model) or liquid/solid contact area (Cassie-Baxter's model), and water contact angle (CA) on a smooth surface of the same material [12, 13]. For the Wenzel state, the wetting behavior is such that the liquid fills the roughened surface completely, due to strong liquid/solid interaction. For the Cassie-Baxter state, the wettability of a surface is affected by a combination of surface roughness and chemical heterogeneity, and the droplet sits on top of the peaks of the roughness with air trapped between the peaks and the droplet. The contact angle of a liquid is the angle formed between the liquid/vapor interface and the liquid/solid interface. Figure 1.1 illustrates the two wetting regimes.

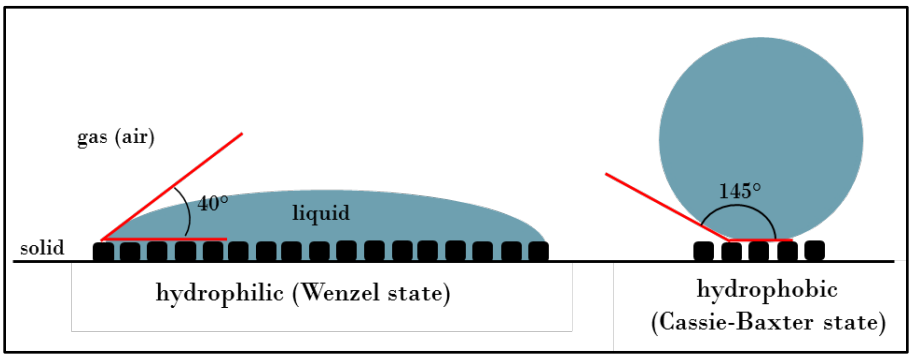

Figure 1.1. An illustration of hydrophilic and hydrophobic wetting behaviors on a textured surface. The Wenzel and Cassie-Baxter wetting modes are shown as well.

The Wenzel and Cassie-Baxter models are frequently referred to in literature for characterization and prediction of the wetting behavior of surfaces [14]. The equation for Wenzel's model is:

$$\cos\theta_r^W = [r^W(geo)]\cos\theta_{smooth}^e \quad (1)$$

where $r^W(geo)$ is the roughness parameter defined as the ratio of the real surface area of the rough surface to the projected smooth surface area, and θ_{smooth}^e is the equilibrium contact angle of a drop on a smooth surface of the same material. The equation for the Cassie-Baxter model is:

$$\cos\theta_r^{CB} = f_1\cos\theta_1 + (1-f_1)\cos\theta_2 \quad (2)$$

where f_1 is the liquid/solid contact area fraction, and θ_1 and θ_2 are the equilibrium contact angles of the same liquid on each of the smooth surfaces of a two-component composite smooth

solid surface of varying heterogeneity. For example, if a substrate was roughened and a surface coating was applied to discrete portions of the surface, equilibrium contact angles would be needed for both materials' smooth surface to calculate the resulting contact angle, θ_r^{CB}. In a simplifying case such as when air pockets are present on a rough single-component surface, the contact angle θ_2 of a water droplet in air is 180°, which makes $cos\ \theta_2$ equal -1. The equation for Cassie-Baxter then becomes:

$$cos\ \theta_r^{CB} = f\ [cos\ \theta_{smooth} + 1] - 1 \tag{3}$$

where f is the liquid/solid area fraction and θ_{smooth} is the contact angle on the smooth, heterogeneous surface.

The drawback to these wetting models is that they are only valid for uniformly rough surfaces where the roughness factor and area fractions are constant [14]. This constancy does not fit the non-uniform rough surfaces of more complicated topographies such as randomized micro/nano-textured surfaces produced in many areas of research.

It is well known that static contact angles (CAs) can be useful for characterizing the wetting behavior of surfaces. Table 1.1 outlines the range of water CA values commonly referred to in literature to compare the relative wetting behavior of surfaces, and they served in this research as references for judging the effectiveness of nano-texturing and surface chemistry to affect surface wetting behavior.

Table 1.1 Reference water CA descriptions used in literature.

Wetting Regime	Water CA (θ)
Superhydrophilic	$0° \leq \theta \leq 10°$, within 1 s of initial wetting
Hydrophilic	$11° \leq \theta \leq 89°$
Neutral	$\theta = 90°$
Hydrophobic	$91° \leq \theta \leq 149°$
Superhydrophobic	$150° \leq \theta \leq 180°$

The five wetting regimes shown in the table are defined according to generally accepted standards in literature. A surface is said to be superhydrophilic if it attains a water CA of 10° or less within 1 s of the initial wetting. A hydrophilic surface is one that achieves a water CA within the range of 11° and 89°. The surface is said to become more hydrophilic as the CA is decreased from a larger angle. The neutral wetting behavior describes a surface that achieves a water CA of 90°. The neutral designation does not infer that the surface has no surface energy, but indicates that the surface is characterized as residing between the most hydrophilic (0° water CA) and most hydrophobic (180° water CA) wetting behaviors. Hydrophobic surfaces are ones that attain a water CA between 91° and 149°. Superhydrophobic surfaces are those that achieve a water CA between 150° and 180°.

The wide acceptance of the descriptions for water CAs listed in Table 1.1 has led to the adoption of similar descriptions for the wetting behavior related to oil, with a few exceptions. The descriptions of the oil wetting regimes are listed in Table 1.2. The wetting behaviors defined in the table will serve as a common reference for understanding the literature results related to oil wetting in chapter 2 and the oil CA results achieved in this research.

Table 1.2 Reference oil CA descriptions used in literature.

Wetting Regime	Oil CA (θ)
Superoleophilic	$0° \leq \theta \leq 10°$
Oleophilic	$11° \leq \theta \leq 89°$
Neutral	$\theta = 90°$
Oleophobic	$91° \leq \theta \leq 149°$
Superoleophobic	$150° \leq \theta \leq 180°$

1.1.3 Surface Nano-Texturing

Nano-tubes, wires, particles, crystals, pores, rods, gratings, and disks have been added to the growing list of surface nano-structures that are receiving increased interest from researchers [15]. A variety of methods are implemented to apply these structures to the surfaces of materials. Nano-particles, for example, are commonly used in a sol or colloidal suspension of solid particles in a liquid medium and the specimen is dip-coated into the solution to achieve surface nano-texturing [16-18]. Colloidal suspensions may also be applied by a dynamic method such as spin coating [19, 20]. During spin coating, the principle means of arranging the nano-particles is one of self-distribution and self-assembly on the surface of the spun materials. Other methods such as physical and chemical vapor deposition processes are also employed to produce surface nano-particles [21, 22].

Ion bombardment of photoresist-coated substrates to create patterned nano-surfaces has grown in popularity in recent years. E-beam and ion beam are dry etching techniques that have been adapted to generate very small feature sizes which are otherwise difficult to obtain from

traditional light-based resist patterning. Nanodots, quantum dots, nano-particles, and nano-pores are successfully produced on surfaces using these techniques [23-27]. Imprint and particle-assisted soft lithography techniques are methods used to create nano-patterned surfaces [28, 29]. These nano-surfaces are fabricated primarily on polymer-based materials.

Wet etching techniques figure very prominently as cheap, effective means of generating nano-topographies on certain material surfaces. Ti, Cu, Al, and Si are examples of commonly etched materials that benefit from these methods [30, 31]. A number of different etching techniques are used such as drop, electrochemical, electrolytic, immersion, rinsing, and wipe etching—each with its advantages and disadvantages [32]. Many of the wet etching procedures developed for nano-texturing are brought about by experimental trial and error and empirical observations carried out over long periods of time. Of these different types, wet etching without the aid of an external electric current is the oldest and most used technique for micro/nano-texturing. This type of etching works by chemically-attacking the crystal structure and grain boundaries and dissolving the defects of the specimen being etched, thus creating textured surfaces. Because etching processes have many variables and the results are specific to the specimens being treated, there are literally hundreds of variations on any particular approach. The types of topographies generated using etching techniques are seemingly endless, as well.

A very different approach to nano-texturing is made possible by using the crystallization of amorphous silicon (a-Si). The discovery and development of a-Si as a nano-texturing material is outlined in the following sections.

1.1.4 Crystallization of a-Si

Crystallization of a-Si has many applications. One of those applications is in solar cell technology. Thin film solar cells which could be produced on low-cost substrates were of prime interest to various researchers [33-35] who were focused on finding economically viable alternatives to the high cost of the pure, single-crystal Si approaches. Metal-induced crystallization of a-Si was created as a cost-effective means of producing polycrystalline silicon on a large-scale [36]. Metals such as Al, Au, Ag, and Ni were used to lower the crystallization temperature to efficiently convert cheaper, lower quality a-Si to higher-quality polycrystalline form [37].

Al-induced crystallization (AIC) is a widely studied method of metal-induced crystallization. AIC of a-Si technique began as a method of producing large poly-silicon grains for use in semiconductor, electronic, solar cell, and photovoltaic applications [38]. Al placed into contact with a-Si significantly lowers the crystallization temperature of the a-Si/Al mixture below the eutectic temperature of 577°C [39, 40]. Crystallization temperatures as low as 150°C [41] have been achieved in producing large-grained poly-silicon films used in devices such as solar cells and thin film transistors [42]. Lowering the crystallization temperature can also facilitate the production of textured surfaces on materials that cannot withstand high temperature.

The development of a faster AIC of a-Si process was the aim of a few researchers. AIC of a-Si parameter variation was studied extensively by the Klein group for affecting the grain size, density, and crystallization time [40]. The experiments were aimed at determining the most efficient approach to synthesizing certain grain sizes while reducing the processing time. They found that the combination of a temperature profile implemented during annealing and

modification of the Al layer thickness were successful for maintaining a fixed grain size while reducing the process time by about 30 min.

1.1.5 Rapid AIC of a-Si

The production of small, nanometer-sized grains of polycrystalline Si was a departure from the large-grained features usually generated by the AIC of a-Si technique. To create them, higher annealing temperatures and shorter annealing durations were implemented by the Zou group. Their approach limited the grain growth of a-Si while creating more nucleation sites for nano-textures. Methods developed by Zou et al. successfully produced nano-textured surfaces on silicon substrates using rapid AIC of a-Si [43]. Their research also led to the study of the effect of a-Si thickness on the formation of aligned silicon nanostructures such as silicon nano-wires, nano-crystallites, and nano-particles [44, 45]. AIC of a-Si was being used by their researchers to generate surface nano-texturing processes on glass and Si substrate to achieve superhydrophobicity and superhydrophilicity for potential applications such as microfluidic channel creation, anti-fogging, and self-cleaning surfaces [46, 47].

1.2 Motivation

The AIC of a-Si process has been studied on stainless steel metal [48]. It is also desirable to extend the study to other widely-used metals, such as Cu. Cu is a very popular metal found in many architectural, engineering, commercial, and industrial applications. A widely-used material such as Cu that possesses controllable wettability and a low coefficient of friction (COF) could have many uses. Some potential uses include non-stick surfaces for food preparation, reduction of heat exchanger fouling in hydronic heating and refrigeration systems,

and reduction in fluid flow friction in machinery components made from Cu. Other uses might include addressing lubricant retention and migration issues that affect wear and friction in components such as seals and bearings.

Preliminary experiments on Cu were performed to develop the AIC of a-Si process parameters and demonstrate the repeatability of generating similar nano-topographies [49]. More research is still needed on the AIC of a-Si process for Cu to understand the impact that various parameters have on nano-texture formation. In particular, the effect of changing the a-Si film thickness needs to be investigated. The process annealing conditions also contain variables that need further study to comprehend fully their effect on both nano-texture generation and surface wetting behavior. The properties of nano-topographies to facilitate the retention of lubricants need to be explored for a wider variety of surface wetting possibilities. Finally, a friction study of nano-topographies needs to be performed to address a need for friction reduction for various engineering applications involving Cu. These studies constitute this thesis research.

1.3 Organization of the Thesis

The thesis is organized into 5 chapters. Chapter 1 is an introduction to the thesis that provides information describing the size-dependent properties at the nanoscale, surface wetting properties, a brief overview of surface nano-texturing, and the development of crystallization of a-Si. Chapter 2 is a comprehensive review of literature that discusses nano-topographies on Cu substrate fabricated by wet etching techniques, oleophilic and oleophobic nano-topographies generated on different substrates, COF testing of nano-topographies using the TriboIndenter, atomic force microscope (AFM), and scanning probe microscopy (SPM), and current research on

the AIC of a-Si technique. Chapter 3 discusses the experimental details of the work performed for the thesis such as how the AIC of a-Si process was implemented, a description of the method used to test surface wetting, and the friction testing procedures that were applied to nano-textured Cu substrate to create the COF results. Chapter 4 provides the research results and discusses the observations made during surface wetting and COF testing on the nano-textured surfaces fabricated using AIC of a-Si on Cu substrate. Lastly, chapter 5 presents the conclusions of the research and the goals that were achieved, as well as future work for producing nano-topographies on Cu substrate.

CHAPTER 2

LITERATURE REVIEW

2.1 Micro/Nano-Texturing and Surface Wetting on Cu Substrates

Nano-surface engineering to increase the hydrophobic and hydrophilic wetting properties of Cu has not been well studied. As was the case for micro-texturing, chemical etching remains the primary method to produce nano-topographies on Cu. The success of chemical nano-texturing methods rely predominantly on the application of etchants to dissolve dislocation sites on the surface of metal substrates, resulting in the roughened surfaces which are necessary to achieve hydrophilic and hydrophobic surfaces. For instance, Cu alloys have been etched with nitric acid and hydrogen peroxide to roughen the substrate to enhance its hydrophobicity [30].

For another application of etchants, Shirtcliffe et al. created a photolithographic mask to pattern photoresist that was spun onto Cu (99+ wt. %) samples [50]. After patterning and developing of the photoresist, 5 μm – 40 μm hemispherical pits were etched anisotropically into the substrate using 0.9 M potassium persulfate solution. Hydrophobization occurred with the aid of a fabric waterproofing solution (Extreme Wash In, Granger) and heating the samples for 20 h. The 30-μm pattern achieved a water CA of 155 ± 3° after further roughening by a second etching treatment.

Recent research conducted to increase the hydrophobicity of a Cu-Zn alloy (Cu 76 wt. %, Zn 24 wt. %) used a one-step, wet chemical approach that used dodecanoic acid as an etchant and a glass slide to cover the treated area [51]. Covering the alloy with a glass slide accelerated the creation of flower-like superhydrophobic surfaces on the Cu-Zn alloy by changing the local

oxygen concentration and formation of oxygen difference cells. An immersion time of up to 3 days of the alloy in the etching solution was required. A water CA of 161° was achieved with this approach.

Another wet chemical approach was used by Liu and associates to create superhydrophobic surfaces on polished Cu (99.5 wt. %) substrate [52]. The polished Cu substrate was immersed in an oxalic acid aqueous solution of 0.5 wt. % concentration. This method involved immersion times of up to 7 days of the alloy in the etching solution, followed by surface modification using spin-coated Poly Dimetysiloxane Vinyl terminated (PDMSVT) and oven annealing at 120°C. Micro- and nano-particles of 0.5 μm and 100 nm average diameters, respectively, were cited as contributors to the 154° water CA and 4° sliding angle obtained.

More recently, the application of a hydrolyzed solution of perfluorooctyl-trichlorosilane, or FOTMS, was used in a reaction with Cu surfaces to attain a low surface energy [53]. Cu (90 wt. %, Zn 10 wt. %) was immersed in NaOH, HCl, and tolulene for 5 days to produce a micro/nano-surface morphology which resembled clusters of microspheres topped with nano-particles. The microspheres were 1.5 μm – 3 μm in diameter and the nano-particles were 50 nm. The samples were immersed in FOTMS solution for 3 days duration, with the result of a maximum water CA of 155.3° and sliding angle of 3°.

Combined micro- and nano-topographies were used to achieve a superhydrophobic surface with an ultra-low roll angle on the surface of Cu [54]. Cu (99.9 wt. %) samples were first subjected to sandblasting media with an average particle size of 425 μm to generate a micro-topography. 106 μm and 180 μm-sized sands were then used to create uniform nanoscale villous films on the micro-texture. Oxidation of the sandblasted surfaces was achieved by immersion of

the samples in 0.065 mol/L potassium persulfate and 2.5 mol/L potassium hydroxide solutions. Superhydrophobicity was facilitated by immersing the samples in 0.8 g of fluoroalkylsilane (FAS) dissolved in 50 g hexane and distilled water and heating the samples at 250°C for one half hour to allow the samples to become fluoridized. Petal-like nanosheets occurred on the surface of Cu, resulting in a maximum water CA of 161° and roll angle of 1° after 0.5 h fluorination.

Some of the wet chemical techniques demonstrated an ability to change the surface wetting properties of Cu from superhydrophilic to superhydrophobic. A drop-etching method utilized 0.05 M phosphoric acid dropped onto Cu (99.9 wt. %) foil which produced a blue film from galvanic cell corrosion after 36 h [55]. The film was collected and placed in a HNO_3 solution to synthesize Cu phosphate dihydrate. The film contained porous dendritic crystal nanosheets that were about 80 nm thick and were oriented perpendicular to the substrate. Following drying at 80°C overnight, the wettability of the surface was characterized as superhydrophilic, or having a water CA of 2° ± 1°. Then, the blue film surface was deposited with a 5 nm Au film and immersed in 1 M n-dodecanethiol for 2 h to permit formation of a self-assembled monolayer. After drying at 80°C overnight, the water CA was found to be 155.5° ± 1°, therefore switching the superhydrophilic nano-surface to a superhydrophobic one.

The creation of superhydrophilic surfaces on Cu substrate is a relatively new area of research. Highly-wetting surfaces using $Cu(OH)_2$ as a basis were successfully created. Superhydrophilic $Cu(OH)_2$ nanowires were produced by a solution-immersion process using aqueous sodium hydroxide and potassium persulfate [56]. The nanowires formed network-like interconnections on the surface of the immersed Cu plate. The intended direction of this research, however, was the fabrication of superhydrophobic surfaces on engineering metals—not superhydrophilic ones. Similarly, membrane formations featuring nano-belts and "stick bundles"

were types of nano-surfaces created from modification of $Cu(OH)_2$ [57]. Reduction and hydration reactions on $Cu(OH)_2$ crystals were used to create Cu_2O and CuO membranes that were composed of close-packed nano-particles. The membranes were shown to possess superhydrophilic properties.

Researchers irradiated Cu to produce highly wetting surfaces for improvement in critical heat flux (CHF) related to pool and nucleate boiling [58, 59]. A superhydrophilic surface was created by exposing TiO_2 deposited on Cu to ultraviolet light. The TiO_2 crystal surface was reduced to Ti^{3+}, and an oxygen vacancy was created. The oxygen vacancy bonded with H in water molecules from the air, resulting in a hydroxyl group forming on the surface. The surface then acted as a chemisorbed water layer to improve pool and nucleate boiling heat transfer. The superhydrophilic heat transfer nano-surface enhanced the phase change phenomena for more effective boiling and condensing. Nucleate boiling achieved a 30% higher CHF over that of conventional Cu by reducing the water CA, and a heat transfer coefficient 40 times that of conventional Cu was attained by superhydrophilic surfaces for pool boiling.

2.2 Oil Wetting on Various Nano-Topographies

Micro/nano-topographies were created on a variety of commonly-known materials for studies of oil wetting behavior. The creation of superoleophobic surfaces on Si (111) substrates was achieved by coating a Si wafer with Au nano-clusters formed from 0.03 M $KAuCl_4$ in a 10 wt. % hydrogen fluoride (HF) aqueous solution [60]. The metal-assisted etching solution formed (100) pyramidal structures and etched pits on the wafer. Hydrophobization occurred by subjecting the structures to 5 silane solutions and heat treatment at 150°C. By varying its concentration, the etching solution HF/H_2O_2 was used to control the Au/Si contact distance on

the topography. As a consequence, various reentrant geometries were achieved, therefore producing superoleophobic structures that prevented hexadecane from entering the surface. The highest oil CA reading was approximately 150° after a 45 min etch.

A texturing and surface chemistry approach involving applications of etching and conformal nano-coatings was utilized on a Si wafer to achieve oleophobicity [61]. The texture was photolithographically generated and resulted in the formation of arrays of 3-μm diameter pillars that were 7 μm high. Oleophobicity was obtained by chemically-modifying the textured surfaces with coatings of fluorosilanes tetrahydrooctyltrichlorosilane (FOTS), octadecyltrichlorosilane (OTS), and polytetrafluoroethylene (PTFE). Hexadecane was shown to achieve 116° oil CA when modified with PTFE and paired with the textured surface and 158° oil CA when modified with FOTS and paired with the textured surface.

Another approach to create superoleophobic surfaces on Si (100) wafers was thermally growing nano-structured amorphous silica to a thickness of 400 nm and subjecting it to ion track etching [62]. Anisotropic etching of the tracks also occurred through the use of 1% vol. HF aqueous solution. Oleophobization of the nano-surface was achieved by grafting it with perfluorooctyltrichlorosilane vapor molecules under low pressure for 10 h. Various alkanes such as hexane, octane, decane, and hexadecane were tested to illustrate the results on static oil CA from liquids with different surface energies. Hexadecane had the best oil CA result as it exhibited an oil CA of 120° on the nano-surface which was a significant improvement over the 66° oil CA reading on a smooth Si surface.

Superoleophobic surfaces were formed by immersing Ti plate in 0.1 M NaCl etching solution for 1 h to form a micro-texture [31]. Another patterned micro-texture was created by laser micromachining on Ti for a comparison to etching. Anodization of both micro-textured

surfaces resulted in the formation of nano-patterned TiO_2 nanotube arrays on the micro-textures. Dip coating in perfluorooctyltrichlorosilane and n-hexane along with oven heating at 100°C for 0.5 h resulted in superoleophobic surfaces. Hexadecane and glycerol were tested on the fabricated surfaces and the maximum oil CAs achieved were 156° and 155°, respectively. The wettability of Ti surface was changed to superoleophilic by exposing the micro/nano-textured surfaces to UV illumination for 90 min.

For Al substrate, both sandblasting and electrolytic etching were used to create oleophobic micro- and nano-topographies [63, 64]. Al_2O_3/30 grit sandblasting media was used to form an initial microscale roughness on the substrate and was followed by submersion of the sandblasted surface in H_3PO_4 etchant to create the nanoscale roughness. The average sizes of the micro- and nano-features were 100 μm and 30 nm, respectively. A low surface energy Al substrate was desired to generate a superoleophobic surface, so 0.1 mol/L Heptadecafluoro-1,1,2,2-tetrahydrodecyltrimethoxysilane (HDFS) solution was applied as a chemisorbed monolayer to the surface nano-topography. The oleophobic characteristic of the surface was verified by an oil CA of 140° using hexadecane.

Oleophilic and oleophobic properties of micro/nano-topographies were studied on materials such as Al, Ti, and Si, but no report has been found on Cu.

2.3 Research Using AIC of a-Si for Surface Wetting

A superhydrophobic surface was prepared on Si wafer using AIC of a-Si to examine the potential of the process to achieve an increase in hydrophobicity without the addition of a low surface energy coating [65]. An a-Si film of 100 nm thickness was deposited on a wafer using plasma-enhanced chemical vapor deposition (PECVD) and left exposed to air for 3 days. Thermal evaporation of 840 nm thick Al was carried out on the samples and oven annealing occurred using temperatures between 500°C and 850°C for 5 s to 10 min duration. After etching, nano-textured surfaces featuring various sizes of island-like nano-particles formed on the surface of the wafer. The sizes varied between 20 nm to 700 nm laterally and 420 nm to 620 nm vertically. Water CA testing was used to assess the improvement in hydrophobicity of the samples. The largest water CA measurement was 137° and the smallest was 80°, meaning that although the lowest water CA was hydrophilic, surface texturing via AIC of a-Si produced a 30° increase in water CA reading over bare Si. The percentage of coverage of the surface with nano-textures was also found to correlate with the surface wetting results.

A hydrophobic surface fabricated using AIC of a-Si and an OTS monolayer was studied to demonstrate the ability of a nano-topography to achieve increased hydrophobicity and even superhydrophobicity when a low surface energy coating was applied [46, 66]. For the study, a-Si thickness was modified in 100 nm increments, beginning with 100 nm and ending at 400 nm. The Al film thickness was held constant, while the annealing temperature was changed from 750°C to 850°C. The control sample, a smooth Si wafer with a thermally-grown oxide on its substrate, achieved a water CA of 112°. The highest measured water CA of the micro/nano-textured surface was 155° and was obtained for the 300 nm a-Si thickness and annealing condition of 750°C/10 s.

A useful characteristic of a-Si is its hydrophilic behavior on a smooth surface, regardless of the substrate on which it is deposited. Amorphous silicon has a water CA of about 60°, but when combined with surface roughness, can exhibit very hydrophilic—even superhydrophilic tendencies. Non-textured glass slides with an inherently low water CA of 15° were studied to produce very stable superhydrophilic surfaces using AIC of a-Si [47]. For this study, the slides were cleaned using a plasma asher and subsequently deposited with an a-Si film thickness of 100 nm. They were then deposited with an Al film of 670 nm thickness. The slides were oven annealed for 10 min duration at 450°C, 550°C, and 650°C. Wet selective etching of the excess Al after annealing allowed the nano-textures generated by AIC of a-Si to be exposed. The surface roughness that was created by nano-texturing, combined with the hydrophilic nature of crystallized a-Si, was cited as reasons for the achievement of stable superhydrophilic (4.3° water CA) conditions on the glass substrates.

Creation of superhydrophilic surfaces on stainless steel substrates was likewise successful using AIC of a-Si [67]. An a-Si film thickness of 300 nm was deposited on the substrate and was overlaid by an 850 nm thick Al film. An annealing profile that ramped temperature up from 400°C to 450°C during 1 h was used. The samples were etched to remove the excess Al after annealing, thus revealing the nano-topography. Evidence of the strong capillary effect, which resulted from the highly-energized surface of silicon nano-crystallites, was apparent after water droplets placed on the sample quickly spread over it. The water CA achieved on the surface was essentially zero after 0.5 s. Interestingly, after treatment of the surface with dip-coated OTS, the water CA became 145°, thus showing that the superhydrophilic surface could be easily converted to a very hydrophobic one.

2.4 COF Analysis of Nano-Textured Surfaces

Studies of the COF of nano-textured surfaces were conducted by various researchers to understand the issues that affect surface contact at the nanoscale. A number of different surface characterization instruments such as AFM, SPM, and nano indenters were employed for the task of generating nanoscale contact on roughened and chemically-modified surfaces. An investigation of nanoscale contact on un-textured Si wafers and those textured with diamond-like carbon (DLC) film and an OTS monolayer was performed to study the most effective method to reduce adhesion and COF [68]. Si_3Ni_4 tips of radii 15, 22, and 50 nm were mounted on the SPM to be used for nano-friction force testing. The 1 μm thick DLC films were deposited on Si wafers with the plasma-assisted chemical vapor deposition technique and the OTS was deposited by a coating process that included oxide etching for surface roughness. The water CA measurements taken on the surfaces of Si, DLC, DLC-impregnated tungsten, and OTS-coated Si varied between 22° and 100°. COF tests were performed with applied normal loads of 0 to 40 nN in 30% relative humidity. It was found that COF decreased significantly for the OTS monolayer samples due to the lower work of adhesion facilitated by the capillary force reduction between the tip and surface.

The COF performance of micro/nano-topographies produced by spin-coating colloidal silica nano-particles on Si (100) substrates was studied using a TriboIndenter [69]. Micro-textures as large as several microns in width and about 100 nm high were formed by the aggregation of nano-particles during spin coating and annealing at 900°C in N_2 for 2 h. The diameter of the nano-particles was approximately 200 nm. The TriboIndenter's 100-μm radius diamond tip was slid along the surface of the textured silica at 0.4 μm/s under applied normal loads between 10 μN—500 μN. The nano-textured surface had the lowest COF because of the

reduced radii of curvature of the individual nano-textures and the reduced surface coverage of silica nano-particles. An 88% reduction in COF was achieved over that of thermally grown oxide on a Si wafer.

The tribological properties of nano-patterned polymeric surfaces were investigated, as well. The polymeric material used in these studies was Poly (methyl methacrylate) or PMMA, a material used predominantly in MEMS device fabrication. One approach for patterning involved soft lithography and direct molding of a thin polymer layer in the void spaces of an elastomeric mold [3]. After curing, the pattern was tested for its friction properties using an AFM that featured a 1.25 μm borosilicate ball as a tip operated in a relative humidity of 45%. Lower COF values were reported than those of un-textured PMMA thin film. Likewise, Brushan et al. used polymeric nano-patterning and a 3.8 μm borosilicate ball as a tip operated in a relative humidity of 50% to study COF of nano-patterned PMMA surface [1]. Micro- and nano-scale scan sizes of 50 μm and 2 μm, respectively, were used. It was found that the nano-structured samples experienced decreased COF due to decreased contact area between the tip and textures, and that there were scale-dependent effects that affected COF as the scan tip and surface interface changed with size.

The tribological study of Ni using nanodot-patterned surfaces (NDPS) produced COF results from applied normal forces ranging between 0 and 300 μN [70]. The investigation explored the elastic and permanent deformation behavior of nanodots subjected to increasingly larger loads. A TriboIndenter featuring a 100-μm radius diamond tip was used to perform the COF tests on both Ni NDPS and the control surface, Si (100). The maximum reductions of COF at low and high loads, respectively, were 83% and 39%. Scanning electron microscopy (SEM) images and AFM measurements showed that under low loads, the nanodots deformed and that

friction force was proportional to real contact area on the nanoscale. The research further illustrated the shearing and removal of nanodots from the substrate as the normal load exceeded 150 μN while maintaining a COF of 0.5.

AIC of a-Si yielded promising results in terms of nano-topography creation and COF reduction. Using a-Si film thicknesses between 100 nm and 400 nm and an Al layer 800 nm thick on Si wafers, nano-textures were created by elevating the annealing temperatures above those traditionally used for the AIC of a-Si process [71]. For COF testing, the TriboIndenter was outfitted with a 100-μm radius tip and operated in a relative humidity of 40%. The applied normal loads ranged from 75 μN to 1500 μN and the scratch length of the tip was 8 μm. The nano-textured surfaces exhibited smaller COF readings than smooth Si under all tested loads, achieving reductions as high as 75% for the 75 μN load and 52% for the 1500 μN load. AIC of a-Si was also used in conjunction with an OTS-modified nano-topography for COF testing of a hydrophobic surface [66]. The nano-textured surface gave the best performance for adhesion tests. The OTS-modified smooth Si surface, however, achieved a 75% reduction in COF over the smooth Si oxide control surface.

2.5 AIC of a-Si on Cu Substrate

Recently, preliminary experiments on Cu were performed to develop the AIC of a-Si process parameters and demonstrate the repeatability of generating similar nano-topographies [49]. A number of pitfalls such as oxidation and issues caused by large differences in coefficient of thermal expansion between the Cu substrate and a-Si film were identified and effective solutions were implemented. The earlier research also explored some possibilities of a-Si/Al film reversal for addressing nano-texture adhesion problems.

In this research, the AIC of a-Si technique will be used to generate various nano-topographies on Cu substrate to modify its surface hydrophilicity and hydrophobicity, and therefore control the surface wettability. Also investigated will be the possibility of using nano-topographies as lubricant retainers. Oleophobic/oleophilic nano-topographies have been produced on other metal substrates, but no research has used a nano-topography on Cu for this purpose. Finally, the nano-textured surfaces will be tested for COF using a TriboIndenter.

An important advantage of AIC of a-Si over the one-step, wet chemical approaches is that it can be applied to many substrates—not Cu only. Furthermore, the process could be implemented in a matter of hours rather than days as required by the wet chemical methods. The process is chemically stable over long periods of time, unlike some processes such as UV treatments and oxidation methods that accompany wet chemical approaches. The AIC of a-Si process does not require the significant investment in chemical treatment facilities and safeguards to accommodate large-scale production of nano-textured surfaces that the wet chemical approaches might require.

The AIC of a-Si process provides separate control of the surface topography at both the micro- and nano-scales more so than the other techniques for generating superhydrophilic and superhydrophobic surfaces. While the technique has been shown to be effective in conjunction with photolithographic micro-texturing techniques [72], it is also a candidate for addressing the failings and limitations of other micro-texturing techniques currently being employed. Lastly, the process can be implemented regardless of the crystallographic nature of the specimen or orientation of its surface, therefore providing more uniform coverage and performance.

CHAPTER 3

EXPERIMENTAL DETAILS

3.1 Sample Description

Sheets of flat, mirror-finished Cu alloy, sized 30.5 cm x 61 cm and having a thickness of 20-gauge (0.82 mm), were purchased from McMaster-Carr (Part Number 9821K31). The chemical composition of the alloy (C11000) consists of Cu 99.95 wt. % and O_2 0.03 wt. %. The metal's physical properties were specified as cold rolled annealed temper. To prevent contamination of the metal, the protective film on the polished side of the Cu sheet was left intact until ready for the AIC of a-Si process. The Cu sheet was cut into sections measuring 13 mm x 25 mm to serve as samples to subject to the nano-texturing process. Shown in Figure 3.1 are the Cu samples used in the research.

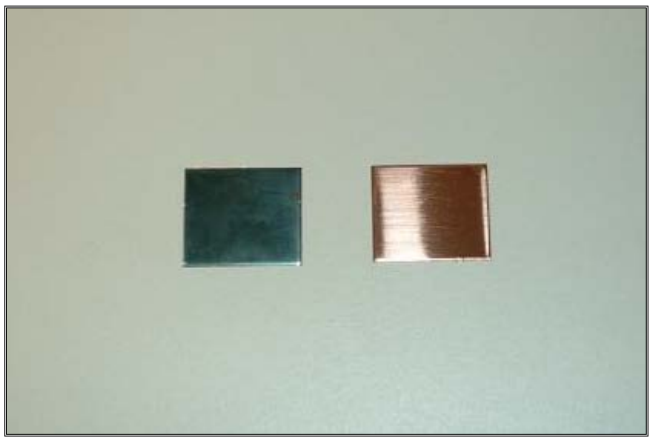

Figure 3.1. The Cu samples used in the creation of nano-topographies. The sample on the left has the protective film intact and the one on the right shows the polished mirror finish with the protective film removed [49].

3.2. Sample Preparation and Cleaning

Removal of the protective film and cleaning the samples was required to eliminate organic contaminants on the sample surface. The samples were first washed with deionized water using moderate spray pressure as a prewash to the solvent treatment. The solvent treatment consists of placing the samples inside a beaker containing acetone and washing them for 20 min using the ultrasonic cleaning apparatus shown in Figure 3.2. Afterward, the samples were cleaned with isopropyl alcohol using the same ultrasonic cleaning procedure for acetone. Isopropyl alcohol dissolved the remnants of the solvent, thus making them easily rinsed away with deionized water. The final 4 min rinsing under a high pressure deionized water spray washed away the remaining isopropyl alcohol residue.

Figure 3.2. Ultrasonic cleaning apparatus used in the preparation of samples for nano-texturing [49].

Drying the samples with N_2 protected the surfaces from oxidation due to standing water. Preservation of sample purity was important for ensuring successful nano-texturing procedures.

Isolating them from airborne contamination by enclosing them in storage cases protected the samples from dust and excess substrate oxidation caused by moisture in the air. Some of the samples proceeded to a-Si deposition, but others were stored in cases under ordinary lab conditions for future processing.

3.3 Process Steps of the AIC of a-Si Technique

Figure 3.3 shows the process steps for AIC of a-Si used in the formation of nano-topographies for the study of surface wetting and coefficient of friction. There were four basic steps that were essential to the AIC of a-Si technique: (1) plasma-enhanced chemical vapor deposition (PECVD) of a-Si, (2) thermal evaporation of Al, (3) annealing of the composite a-Si/Al film on Cu substrate, and (4) selective wet etching of Al. These steps and related processes are described in further detail in the sections that follow.

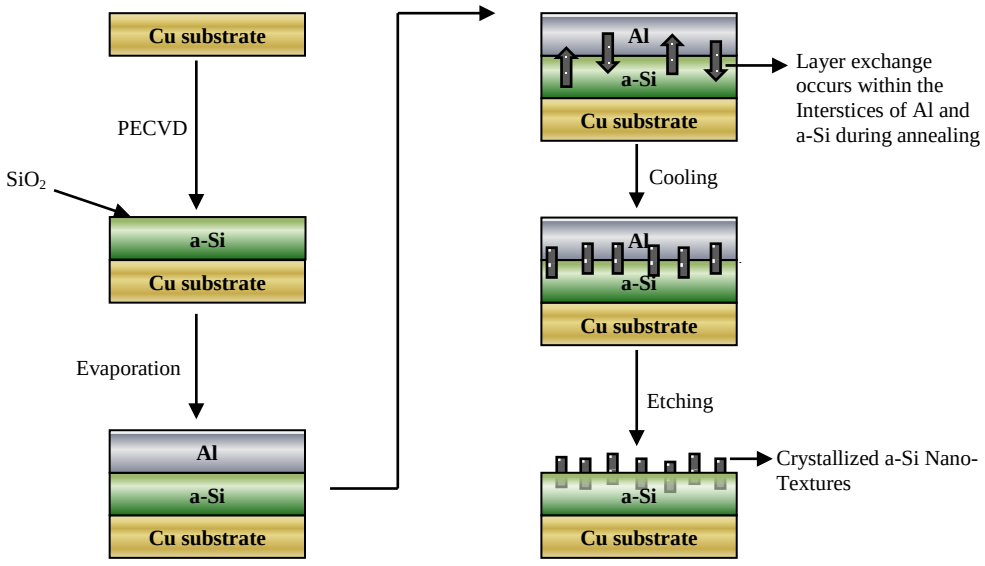

Figure 3.3. The AIC of a-Si process for creating nano-topographies on Cu substrates [49].

3.3.1 Deposition of a-Si by PECVD

Some samples were deposited with a-Si using the PECVD system (Plasma-Therm SLR730) shown in Figure 3.4. Preliminary preparations included flowing the PECVD chamber with N_2 to remove the air trapped inside, followed by the flow of silane (SiH_4) to evacuate the N_2. A vacuum was drawn on the system to remove the SiH_4. To deposit the a-Si film, the PECVD system was operated at an RF power of 20 W, a substrate temperature of 250°C, a chamber pressure of 133 Pa, and a second SiH_4 flow rate of 85 sccm. A plasma reaction was created in the presence of SiH_4, resulting in the deposition of a-Si:H on the sample surfaces. Hydrogenation helped to reduce the number of incomplete bonds inherent to a-Si films and heating the substrate contributed to uniform film layering. The durations needed by the PECVD system to deposit a-Si:H films of 100 nm and 250 nm thicknesses were 4:42 s and 11:45 s, respectively.

Photo courtesy of High Density Electronics Center

Figure 3.4. The PECVD system used in the deposition of a-Si films [49].

After the a-Si deposition process was completed, the samples were removed from the PECVD system, placed inside storage cases, and set aside for a period of at least 48 h at room temperature (25°C) in air. Allowing the 48 h time period was important because growth of a native silicon dioxide (SiO_2) film occurred when the samples were exposed to air. The SiO_2 film aided the adhesion of a-Si to the Al film that would be deposited later. The samples were now ready for Al evaporation.

3.3.2 Thermal Deposition of Al

For the deposition of Al onto the Cu/a-Si substrates, the samples were mounted on a Si wafer using polyimide tape and placed inside the thermal evaporator (Edwards Auto 306) shown in Figure 3.5. The chamber was prepared by filling the system with N_2. N_2 purged the system of air and helped it achieve a high vacuum that, in turn, promoted the deposition of Al. The settings chosen for evaporator operation were a base chamber pressure of 6.65 E-04 Pa, a density of 2.7 g/cm^3, and an Al deposition rate of 4 nm/s. This rate enhanced the uniform deposition of Al onto the Cu/a-Si samples.

Figure 3.5. The Edwards thermal evaporator was used for the deposition of Al onto the Cu/a-Si substrates [49].

The phase change of Al from solid to liquid was aided by passing a 45A current through a titanium boat which held pieces of Al source material. Once vaporized, the buoyant Al migrated toward the wafer located overhead and condensed as a solid on the cooler surface of the samples. A crystal sensor was used to monitor the thickness of Al accumulation on the samples. Two batches, batches A and B, were processed and received 650 nm and 526 nm thick Al, respectively. One critical step which controlled Al oxidation upon contact with air was to allow them to cool inside the evacuated chamber of the evaporator for 10 min duration. Upon removal from the evaporator, the Cu/a-Si/Al samples were identified using sequential numbering and annealing conditions were inscribed using a diamond scribe on their non-film side.

3.3.3 Sample Annealing

The sample annealing procedure consisted of creating an annealing matrix, placing the samples inside the oven and annealing them, and removing them for cooling in air after annealing conditions were met.

3.3.3.1 Selection of the Annealing Matrix

Earlier research confirmed that annealing conditions were important process variables in the formation of surface nano-textures on Cu substrate [49]. To investigate the possibility of creating nano-textures from other annealing conditions, the annealing matrix shown in Table 3.1 was set up. Annealing durations of 5 s, 10 s, and 20 s were chosen as bases to determine the effect of annealing duration on nano-texture formation. The other variable which affected the formation of nano-textures on Cu substrate was temperature. Because Cu (alloy C11000) was

known to have a melting point of 1083°C [73], the annealing matrix temperatures were selected to generate nano-textures well below this point. The addition of Al to the a-Si film was instrumental in assuring the annealing temperatures needed for nano-texture formation would remain below the melting point. Samples from the batches were exposed to temperatures of 650°C, 750°C, and 850°C.

Table 3.1 Sample annealing matrix.

Annealing Duration \ Annealing Temperature	650 °C	750 °C	850 °C
5s	X	X	X
10s	X	X	X
20s	X	X	X

3.3.3.2 Sample Annealing Procedure

After Al deposition, the samples were removed from the evaporator and placed in the annealing furnace (Lindberg/Blue Furnace BF51894C) shown in Figure 3.6. Steady-state operation of the temperature profile was chosen for fast and efficient annealing in accordance

with the rapid AIC of a-Si technique. The furnace was heated to attain the lowest annealing temperature of 650°C to begin, and then progressed higher to 750°C, and finally to 850°C. Annealing durations were 5 s, 10 s, and 20 s for each of the annealing temperatures. Three samples were typically subjected to each annealing condition (i.e., annealing temperature and duration combination), meaning that a total of 27 samples were necessary to complete the annealing matrix.

Figure 3.6. The furnace shown here was used to anneal the samples for nano-texture creation [49].

During annealing, the layer exchange between Al and a-Si occurred and significantly affected the nano-topography formations. Because the annealing process was a major influence in the formation of the different nano-crystalline structures, comprehensive organization of data was necessary to track the combinations of a-Si and Al film thicknesses, annealing conditions, and sample identifications to thoroughly test the AIC of a-Si process for Cu. Upon removal from the oven, the samples were allowed to cool to 25°C in room air.

3.3.4 Sample Etching

The samples were submersed in a non-agitated solution of Transene Al etchant type D at 50°C for 10 min to remove excess Al. The wet bench setup for sample etching is shown in Figure 3.7. The samples were positioned inside an acid-resistant holder and gently lowered into the solution. At 50°C, the rate of etching was known to be 250 nm/min. The 10 min etch duration was sufficient to allow the removal of excess Al from the surface while leaving intact the nano-topographies which were the aim of this research. Delicate rinsing of the samples in several, large beakers of de-ionized water removed the chemical residue left behind by the etching process.

Figure 3.7. This wet bench stored the Transene type D solution for Al etching [49].

The samples were dried using N_2 to avoid the negative effects of water surface tension on the nano-textures and to reduce the potential of oxidation resulting from standing water. Water has a surface tension value of approximately 70 mN/m which can prove detrimental to texture adhesion to the substrate. When the blowing pressure of N_2 was excessive, samples were

allowed to air dry to avoid disturbing those nano-textures which were more fragile. The resulting sample topographies usually exhibited good adhesion and provided ample data to determine the optimum AIC of a-Si conditions for controlling the surface wetting properties of the nano-textured Cu surfaces.

3.4 Sample Characterization

Characterization of the samples was accomplished with the use of SEM and water and oil CA measurements. An accurate analysis of the topographies used in the investigations was important, and these instruments provided recorded evidence of the nano-structures and wetting behaviors that were created.

3.4.1 SEM

The SEM (Philips XL 30), shown in Figure 3.8, was used to verify the presence of the nano-textures which will affect the surface wetting of Cu. Custom-made sample holders were used to mount the samples and position them inside the SEM. The sample holders provided a 45° recline of the sample surface relative to the electron beam. The images of the samples taken in the reclined position enabled the extraction of particle height and width information of the crystallized a-Si for image analysis.

Figure 3.8. The SEM system shown here was used to capture images of the nano-topographies [49].

After mounting the samples, the SEM proceeded automatically through the pump-down and ventilation procedures. A minimum focus magnification of 50k, beam voltage of 10 kV, and about 15 mm working distance from the samples were selected to allow observation of the nano-topographies created by AIC of a-Si. During the image capture, the photo scan rate was chosen to achieve the highest quality. Various images, with magnifications ranging from 500x to 20k, were collected on each sample to ensure an accurate characterization of the nano-topographies.

3.4.1.1 ImageJ™ Characterization of SEM Micrographs

ImageJ™ software was used for particle analysis to determine important characteristics of the nano-topography. This is an open-architecture image processing and analysis software package provided by the National Institutes of Health. An SEM image of a nano-topography that was subjected to particle analysis is shown in Figure 3.9. The analysis software provided a

method of numerically quantifying the data related to nano-texture height and width, particle count, total area of particles, and total area of substrate under consideration. These parameters allowed the calculation of average particle size, particle density, and percent of texture coverage.

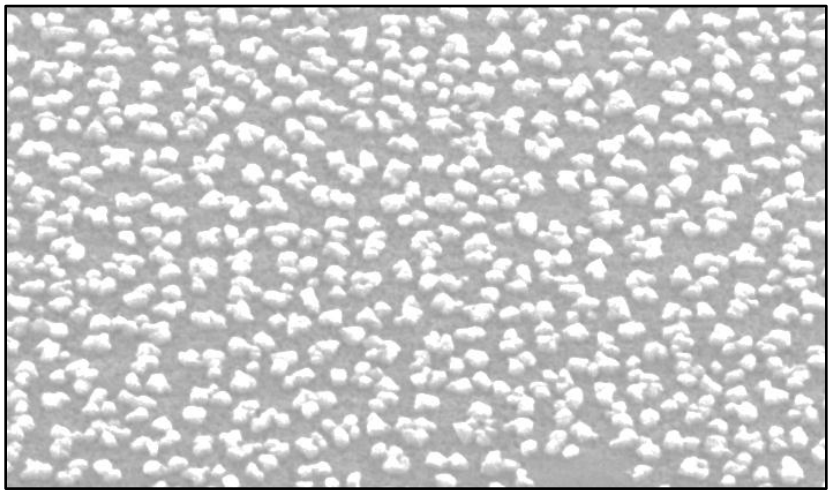

Figure 3.9. An SEM image of a nano-topography created on the sample surface for use in ImageJ™ software to analyze particle formations.

The SEM images were opened inside of the ImageJ™ software where they were scaled for insertion of a new dimension bar and cropped for the deletion of SEM data bar information. Next, the images were subjected to foreground/background color threshold adjustments that produced contrasts between the crystallized a-Si particles and the substrate as shown in Figure 3.10. Threshold measurements were supplemented by specifying the size range of the particles under consideration, usually 5 μm and smaller, using the program's threshold limiter. The highlighted particles could now be parameterized and the important data mentioned previously could be extracted. Image analysis results from multiple samples were recorded and averaged, thus ensuring closely-correlated data from an otherwise subjective analysis method. Microsoft Excel™ software was used to plot the data.

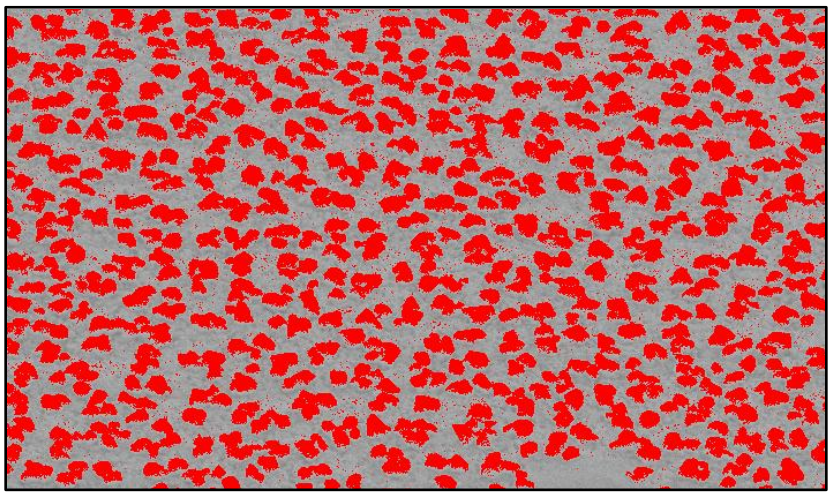

Figure 3.10. ImageJ™ threshold settings were applied to Figure 3.9 SEM image to produce the contrast between foreground and background surfaces for particle analysis.

3.4.2 Water CA

Machine-based water CA measurements afforded convenience in characterization of the nano-topographies' surface wetting behavior as either hydrophilic or hydrophobic. CA measurements using water were obtained for all samples by means of the contact angle machine (DataPhysics Instruments OCA 15) shown in Figure 3.11. To begin, a 500 µL Hamilton syringe was filled with de-ionized water and installed in the machine. The sessile-drop method was chosen to obtain static CA measurements. The dispensed volume for all droplets was selected as 1 µL to promote consistent test criteria and favorable water CA comparisons between batches of samples. To perform the static CA measurement, a droplet was suspended from the end of the syringe needle, the sample was raised using a z-stage to make contact with the droplet and then lowered, and a snapshot of the droplet was taken within 5 s of contact with the surface. An optical image of the droplet was captured at 1.5x magnification using an in-line CCD camera. Imaging was followed by selection of the machine's Laplace-Young calculation feature which

calculated the CA obtained from the captured image. The CA readings of 3 droplets were averaged to obtain a single water CA value and the results were plotted using Microsoft Excel™ software.

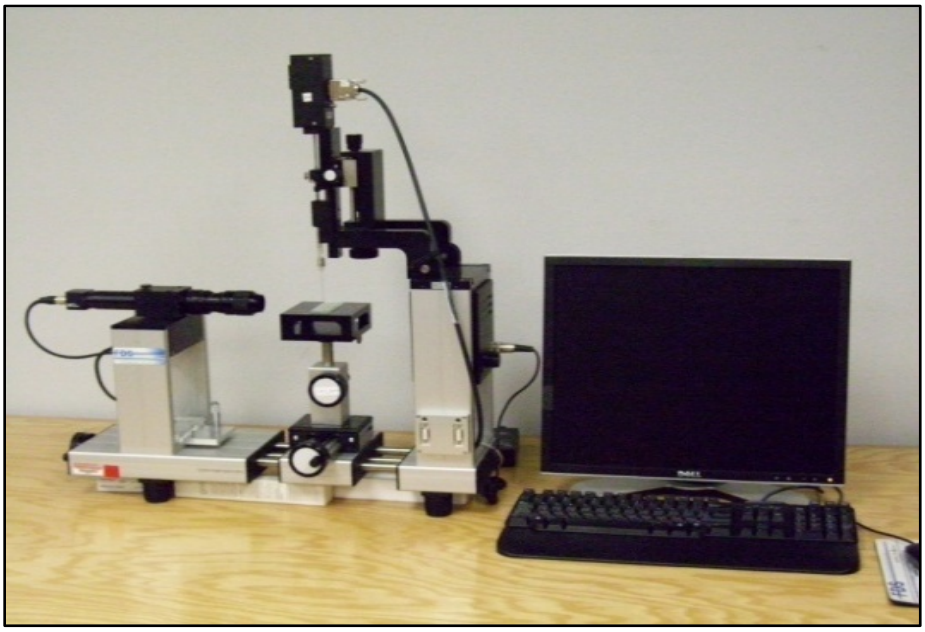

Figure 3.11. The contact angle machine features an in-line camera and power syringe system which dispensed droplets for water and oil CA testing [49].

3.4.3 Oil CA

Surface wetting that incorporated a substance other than water was beneficial for exploring the feasibility of nano-textures to address a wider range of engineering issues than previously investigated. Oil CA measurements were used to assess the oil affinity of the nano-textured samples in comparison to AR Cu. A mineral oil of unknown viscosity and density of 0.8 g/cm^3 was used. The viscosity of mineral oils fall within 20-70 centistokes at 25°C, and its surface energy (35 mJ/m^2) is approximately half that of water. The dispensed volume of the oil was selected as 3 µL to prevent the negative effects of droplet weight on CA measurements.

Since oil possessed a higher viscosity than de-ionized water, a 5 s pause was allowed before taking a snapshot of the droplet to permit stabilization of its flow rate. Otherwise, the image capture procedure for oil CAs was identical to the one for water.

3.5 COF Testing using TriboIndentation

The TriboIndenter™ (Hysitron TI 900), shown in Figure 3.12, was an essential tool to perform the scratch tests which provided data for the calculation of COF. COF testing made it possible to observe whether a reduction in friction occurred as a result of the application of surface nano-textures. COF, usually denoted by μ, is the ratio of the lateral force and applied normal force acting on the TriboIndenters' tip during contact with the sample surface.

The TriboIndenter uses an integrated optical and scanning probe microscope which enables accurate locating and testing of the surface topography under consideration. The resolution for normal force and lateral force are 3 nN and 500 nN, respectively. AR Cu samples as well as nano-textured ones were mounted on the stage of the machine. Sample identification and X-Y-Z calibrations were performed, and the preliminary load-controlling procedures were programmed to prepare the TriboIndenter for scratch testing. For the scratch tests, a diamond tip with a radius of 100 μm was chosen to allow a wide range of load tests while staying within the 12000 μN load limit of the TriboIndenter.

Figure 3.12. The Hysitron TriboIndenter was used in the friction testing of samples.

The load control parameters of the TriboIndenter software are shown in Figure 3.13. In the COF test, the normal load was applied 4 s after the tip had been maneuvered to the test location. The top graph illustrates the ramp-up of the normal load from zero to full force between the 4 s and 9 s time interval. For the following 8 s duration, the tip was slid under full load across the surface of the sample. Afterward, the normal load was ramped downward to zero over a 5 s interval and the tip was withdrawn from the surface 4 s later. The x-direction or lateral displacement control parameters (bottom graph) are also illustrated graphically in the figure. Here, the tip was brought to the test location, and then the tip was displaced 4 μm behind this location. After holding the position for 5 s, the tip was dragged a distance of 8 μm and then stopped. After a 5 s hold, the load was released and the tip was withdrawn from the substrate.

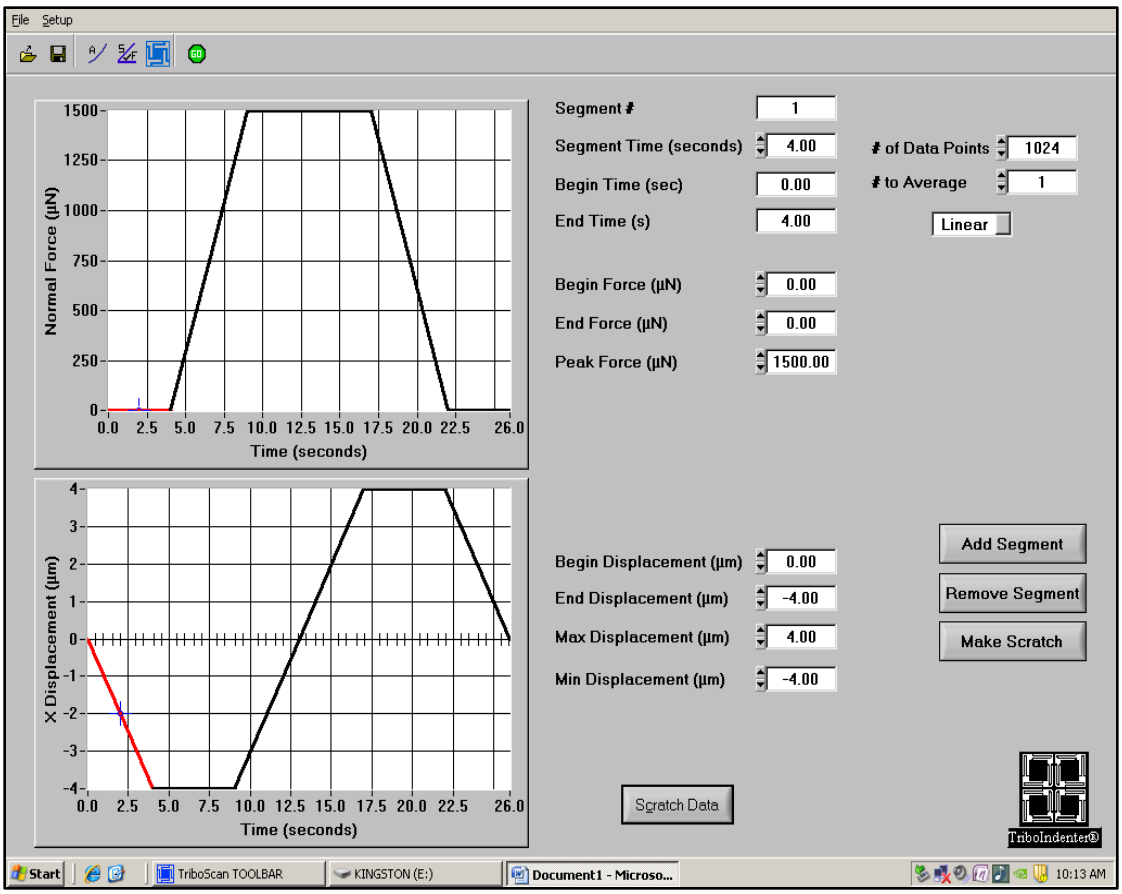

Figure 3.13. The load and displacement control parameters of the TriboIndenter software used to produce the COF results.

The lateral load was measured as the tip was dragged laterally across the surface of the samples during each application of a normal load. Eleven applied normal loads, varied between 50 µN and 10,000 µN, were used for the COF test. A matrix of 55 scratches, performed under the 11 normal loads (each repeated 5 times) was created on the samples. A depiction of the matrix is shown in Figure 3.14. Each scratch was 8 µm in length, and was produced using a lateral tip speed of 1 µm/s. Data for both normal and lateral loads were recorded simultaneously during COF testing and plotted as a function of time. Averaging of the data collected from the scratch matrices permitted the comparison of COF-versus-normal force for the samples.

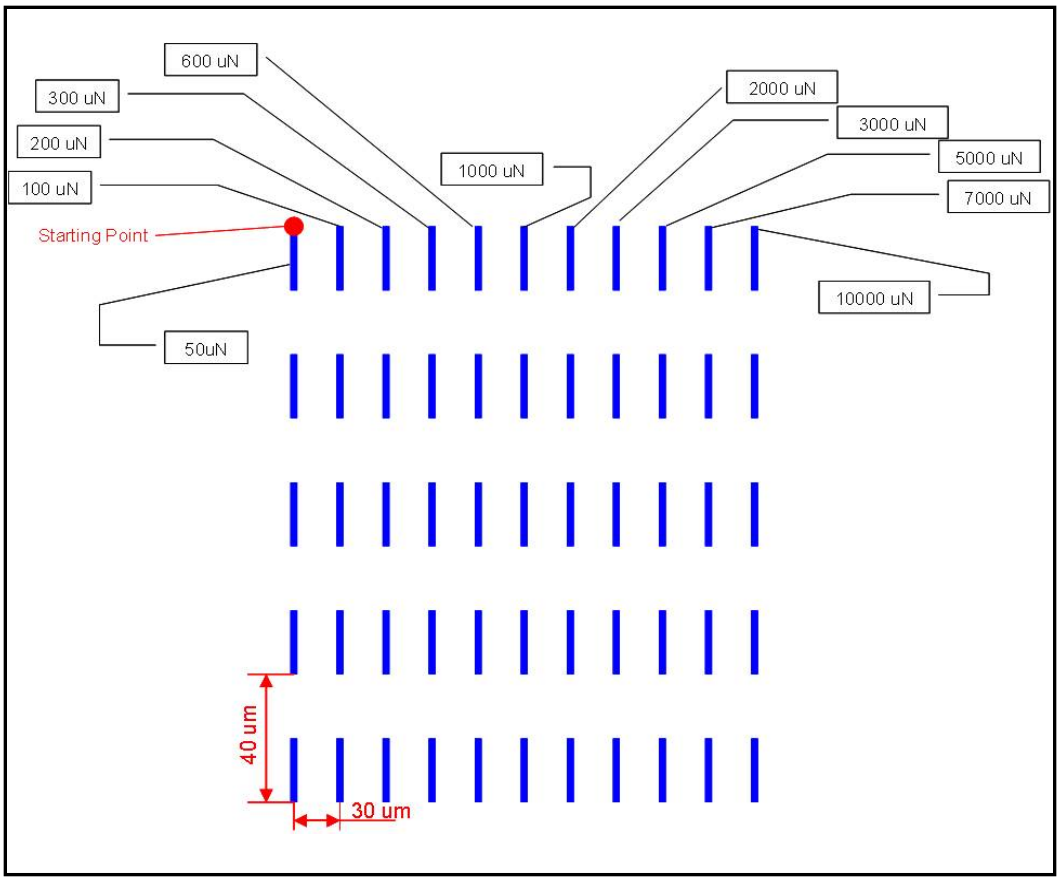

Figure 3.14. Eleven normal loads and the 55 scratches produced from lateral displacements as the tip was dragged across the surface of the samples.

CHAPTER 4

RESULTS AND DISCUSSIONS

4.1 Summary of Experiments

AIC of a-Si techniques were performed on AR Cu substrates for fabricating nano-topographies. The effects of annealing conditions and a-Si thickness on nano-texture formation were studied. Image analysis of the nano-topographies was carried out to obtain data for observing correlations of the batches' annealing conditions and a-Si thickness with respect to texture size, density, and percent of coverage of surface. Water and oil CA measurements were obtained from the nano-topographies to examine the effects of nano-texturing and chemical modification on surface wetting. Finally, the COF of AR Cu and nano-textured surfaces were tested to investigate the potential of nano-textures to reduce the COF.

4.2 Creating Nano-Textures on Cu Substrate using AIC of a-Si

Recently, preliminary experiments on Cu were performed to develop the AIC of a-Si process parameters and to demonstrate the repeatability of generating similar nano-topographies [49]. In this research, results from batch A of the preliminary experiments along with new experiments performed in this study on batch B were analyzed in detail to understand the effect of annealing conditions and a-Si thickness on nano-texture formation. Since neither quantitative analysis of the nano-topographies of batch A nor surface wetting evaluation of the nano-topographies was performed, it is important to reexamine a portion of the earlier research to perform these analyses for the current research. Therefore, for completeness of this thesis, batch

A is described in section 4.2.1. Qualitative analysis of the nano-topographies performed in the earlier work on batch A is summarized in section 4.2.2.

4.2.1 Results of a-Si and Al Film Depositions for Batch A

Batch A consisted of 27 AR Cu samples to be nano-textured using the AIC of a-Si process. Before texturing, the samples underwent ultrasonic cleaning in acetone and isopropyl alcohol to remove contaminants from the sample surface, followed by deionized water rinsing and drying with an N_2 blow. For the initial a-Si deposition, a 100-nm thick film was deposited on the surface of the samples using PECVD. The absence of debris, bubbles, or bare spots on the surface indicated excellent adhesion of the film to the substrate. The processed samples exhibited a greenish hue, yet they appeared uniform in coverage and coloration, indicating a successful application of film to Cu substrates. The samples were put in cases and stored under normal lab conditions for a period of one week to facilitate the growth of the SiO_2 layer occurring naturally on the surface of a-Si films exposed to air.

Rapid crystallization of a-Si was desired for batch A samples. To achieve this objective, an Al layer 650 nm thick was deposited over the a-Si film which enabled a lower crystallization temperature during the annealing step. The composite a-Si/Al film depth totaled 750 nm. Despite the presence of Al and a-Si on the Cu substrate, the coverage remained smooth and uniform, suggesting that film stresses were well-managed during the depositions. A mirror finish was produced by Al on the surface of the samples.

4.2.2 Results of Annealing Duration and Temperature on Nano-Texture Formation

Nine samples were selected from batch A to study nano-textures created using the AIC of a-Si process developed for Cu. These samples were divided according to nine annealing conditions, or annealing temperature/duration groupings. The annealing temperatures were 650°C, 750°C, and 850°C, and each temperature had 3 associated annealing durations of 5 s, 10 s, and 20 s. The samples were characterized using SEM and the images of the nano-topographies that were generated are shown in matrix form in Figure 4.1. The annealing temperature is located on the horizontal axis and the annealing duration is on the vertical axis.

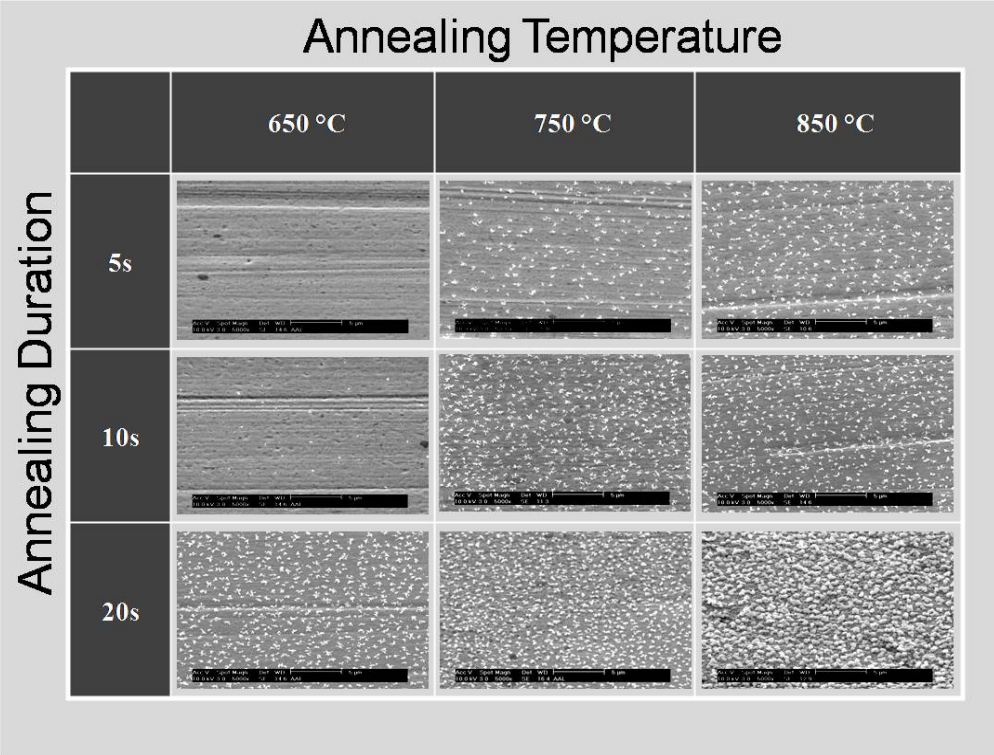

Figures 4.1 Batch A SEM images of Cu samples subjected to AIC of a-Si. The a-Si thickness was 100 nm. The images showed a trend toward increased nano-texture particle density and size as annealing duration and temperature were increased. All images were captured at 5k magnification. The lightly-colored structures are nano-textures [49].

The nano-topographies responded to changes in the annealing duration. Visual inspection of the SEM images showed that longer annealing duration facilitated increases in particle density and size of the nano-textures. This conclusion was evident when using a fixed temperature while allowing the duration to increase and observing the changes in the topographies in Figure 4.1. Clearly, more sites nucleated as the duration increased, thus affecting the size and density of the nano-textures. This trend was easily observed at each annealing temperature.

A similar conclusion could be made for the effect of annealing temperature on nano-texture formation. Modulation of the annealing matrix temperatures revealed that a correlation existed between annealing temperature and nano-texture formation. Visual analysis of the SEM images in Figure 4.1 based on a fixed annealing duration and permitting the annealing temperature to rise from 650°C to 850°C, showed that the number and size of nano-texture formations generally increased as the temperature rose. This trend was observed across all annealing durations. As the temperature increased, particle density and size of the nano-textures correspondingly increased. More thermal energy was transferred to the composite film for crystallization of a-Si, which in turn, produced larger, denser nano-textures. It was also noticed that nano-texture formation was imperceptible at the lowest temperature of 650°C and duration of 5 s, but formations became visible and increased in size and particle density as the annealing temperature increased at that same duration, thus becoming more in line with the trends observed for the other annealing durations.

4.3 Study of Variation of a-Si Film Thickness on Nano-Texture Formation

A study of the effects of a-Si thickness on nano-texture formation was beneficial for gaining a better understanding of the relationship between the AIC of a-Si process variables and the results for surface wetting and COF. A different batch of samples featuring a thicker a-Si layer was created for this purpose. The two batches allowed a comparison of the texture size, particle density, and percent of coverage of surface which resulted from the change in annealing conditions and a-Si thickness, therefore presenting a range of texturing choices for future nano-surface engineering applications.

4.3.1 Effect of a-Si Thickness on Texture Size, Density, and Percent of Coverage

Batch B, shown in Figure 4.2, was created to study the effect of increasing a-Si film thickness on nano-texture formation. Before deposition, the 27 samples in the batch were cleaned ultrasonically as described in section 3.2 to assure that a contaminant-free surface existed. The a-Si layer was then deposited to 250 nm thickness. The processed samples conveyed a bluish hue that was indicative of the thicker layer applied to batch B, yet they exhibited the same uniformity in film coverage as the samples comprising batch A deposited at 100 nm thickness.

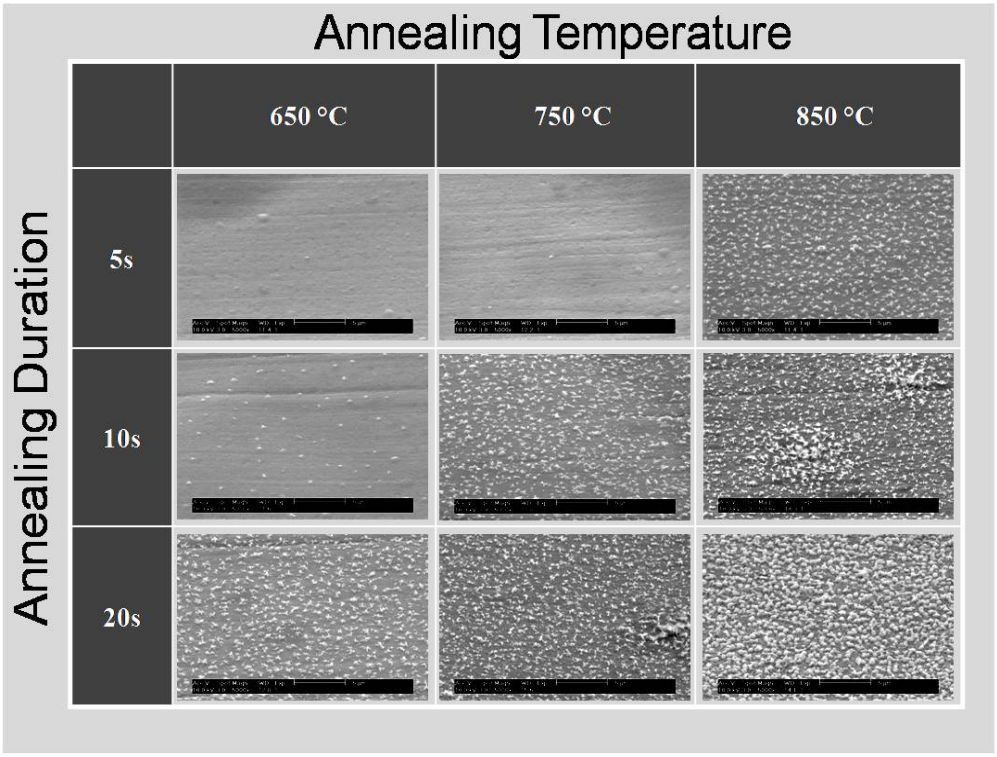

Figure 4.2. The SEM images of batch B Cu samples subjected to AIC of a-Si. The a-Si film was increased to 250 nm. The images showed a trend toward increased nano-texture particle density and size as annealing duration and temperature were increased. All images were captured at 5k magnification. The lightly-colored structures are nano-textures.

During thermal evaporation, the Al film was deposited only to 526 nm. Intentions were to deposit an Al thickness of 650 nm, but it was not possible because of a lack of precise control of the thermal evaporation process. A smooth, mirror finish was obtained on this batch of samples as well, indicating that the composite a-Si/Al film contained negligible effects from thermal stress. Although a difference in Al thickness between batches A and B existed, inspection of data from Si and glass substrates with small inconsistencies in their Al thickness confirmed that any data collected from the batches would not cause serious skewing of results.

After the samples were deposited at their respective a-Si/Al thicknesses, they were annealed in agreement with the matrix conditions outlined in section 3.3.3.1 and wet etched to reveal the nano-textures fabricated on Cu substrates. In short, the nano-textures of batch B showed a trend toward increased texture size and density over those of batch A. The process developed to produce nano-textures on batch B Cu substrates revealed that several factors positively affected the AIC of a-Si process result. Factors such as the thickness ratio of Al -to- a-Si, annealing temperature and duration, coefficient of thermal expansion differences, the initial Al and a-Si layer thicknesses, defect and grain boundary locations, etc., have an effect on crystallization patterns and nano-texture formations. However, focus at this time was limited to those readily controlled during experimentation; namely, a-Si thickness, annealing temperature, and annealing duration.

Figures 4.3a, b, and c are the SEM images of batches A and B arranged side-by-side for comparison of the nano-texturing results achieved by increasing the a-Si thickness from 100 nm to 250 nm. The figures are delineated by annealing duration. Figure 4.3a shows the images of textures fabricated by 5 s duration, 4.3b are those textures fabricated by 10 s duration, and 4.3c contains the images of the textures fabricated by 20 s duration. The annealing temperature changes from 650°C to 850°C in each figure. The results of the SEM images of batches A and B demonstrated qualitatively that the textures generated in batch B were generally larger in size and higher in density than those in batch A. The images of Figures 4.3a-c were used as bases for the quantitative analysis as well.

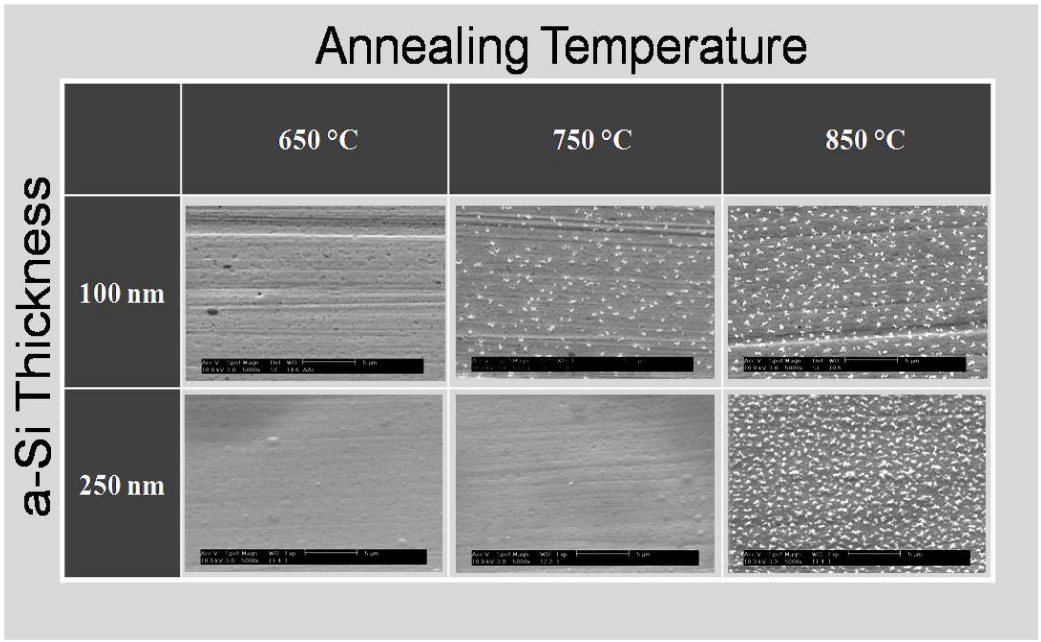
Annealing Temperature
650 °C
750 °C
850 °C
a-Si Thickness
100 nm
250 nm

(a)

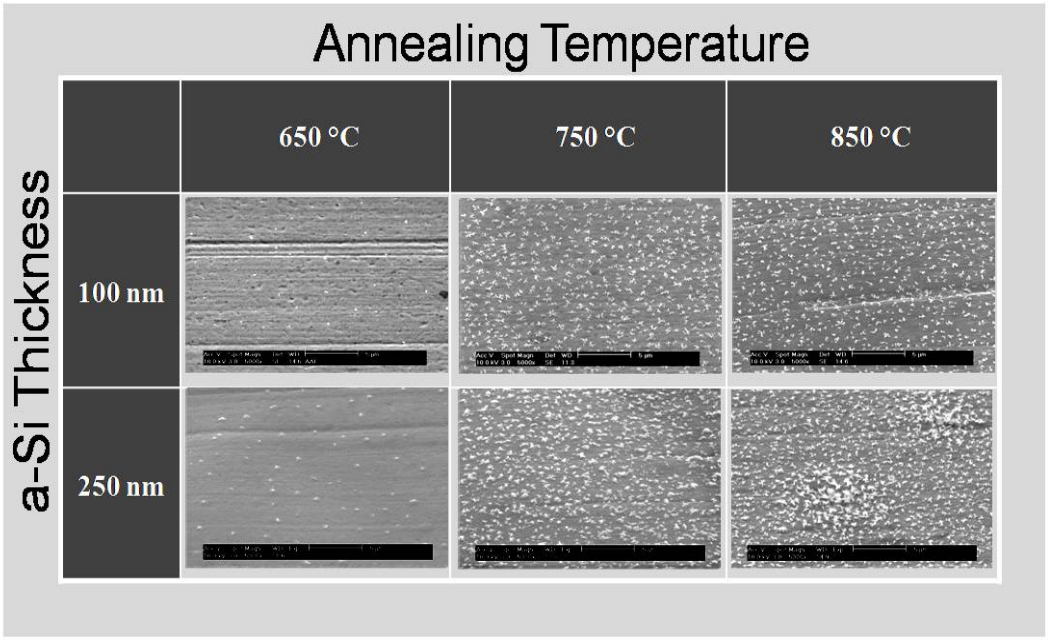
Annealing Temperature
650 °C
750 °C
850 °C
a-Si Thickness
100 nm
250 nm

(b)

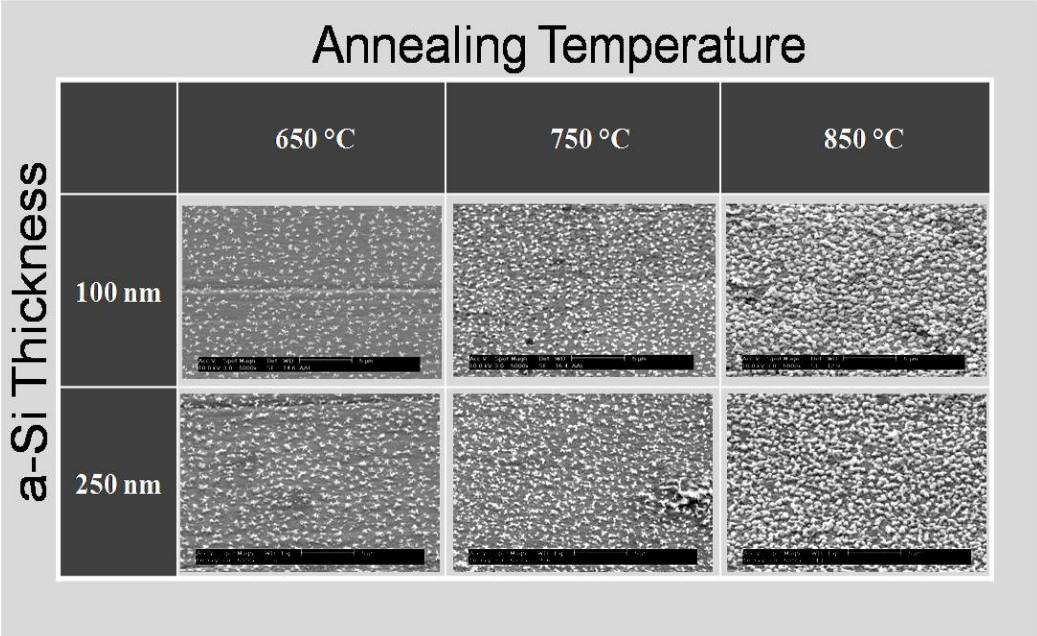

(c)

Figures 4.3a, b, and c. Batches A (100 nm a-Si) and B (250 nm a-Si) texture comparisons for (a) 5 s, (b) 10 s, and (c) 20 s annealing durations. All images were captured at 5k magnification. The lightly-colored structures are nano-textures.

The production of larger, denser nano-textures was not unexpected, considering that batch B possessed more a-Si supply than batch A, therefore providing more opportunity for a-Si crystallization at equivalent annealing conditions. Another reason for the size and density difference was the occurrence of lateral nucleation in batch B. It was deduced that lateral growth was easier because of higher crystallization energy closer to the substrate [30]. Crystallized particles within batch B were suppressed from vertical growth more than ones in batch A due to the presence of a thicker a-Si layer above the particles [24, 33]. The resulting nano-textures of batch B exhibited broader particle formations, while batch A tended toward narrower, but peaked formations.

In Figures 4.4a and b are the SEM images that were obtained for comparison of the two batches' texture geometries. Batch A nano-textures, in Figure 4.4a, featured pointed tops and angular, chiseled surfaces around their sides, likely as a result of the lower a-Si supply and the decreased crystallization potential further away from the a-Si layer [74]. There was no doubt that the peaked geometry of batch A would provide the minimal contact area of the two nano-topographies if another surface was brought into contact with it. The wider particle formations in Figure 4.4b were characteristic of the effects of particle suppression under the thicker a-Si film layer. The engineering benefits of both texture types were apparent. The peaked surfaces could help with adhesion and friction issues, whereas the broader surfaces might be useful for high-load contact and surface wetting.

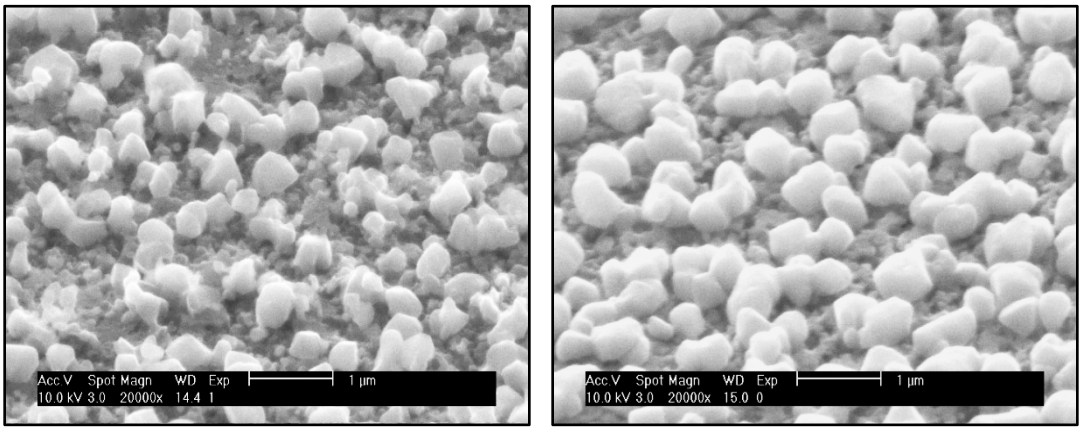

(a) (b)

Figures 4.4a and b. SEM images of (a) batch A and (b) batch B samples that were created from the 850°C/20 s annealing condition. Notice that the textures produced by the thicker a-Si layer of batch B were wider and featured flat tops, proving that the overall geometry of the nano-topography was affected, too. Both images were captured at 20k magnification.

ImageJ™ software was used to produce numerical data to quantitatively evaluate the results inferred by the qualitative analysis of the SEM images. Average texture size, particle density, total number of particles, percent coverage area of nano-texture, and total substrate area were extracted from SEM images of both batches. The data for average texture size, particle density, and percent of coverage—each with respect to a-Si thickness—are presented graphically in Figures 4.5-4.7. The plots were rendered using the log scale on the vertical axis to preserve the clarity of the data for 18 samples and allow trends resulting from the various nano-topographies to be easily observed.

The plots were organized according to the results obtained from the nine annealing conditions summarized in the legends—that is, the annealing temperatures of 650°C, 750°C, and 850°C, and the three annealing durations associated with each temperature, i.e., 5 s, 10 s, and 20 s. The horizontal axis of each graph displays the two a-Si thicknesses of 100 nm and 250 nm. The data points derived from the nine annealing conditions for both batches were aligned vertically under their respective a-Si film thicknesses. To facilitate direct comparison of batches A and B results, the corresponding annealing conditions from each batch were connected via a line. The lines do not imply a linear relationship between the data points of the batches, but serves as a visual aid to help identify like conditions for comparison and analysis. Analyses of the plots revealed some interesting results useful for future nano-surface generation and engineering applications.

The impact of film thickness on average texture size was studied by changing the a-Si thickness. Having captured the SEM images of the nano-texture formations of both batches, the particle analysis function in ImageJ™ software was used to outline the island-like particle formations of the images of Figures 4.3a-c. Data from the analysis was used to calculate the

values for average texture size reported in Figure 4.5. The average texture size was measured in μm^2 and plotted on the vertical axis of the graph, while the a-Si thicknesses and accompanying annealing conditions are shown on the horizontal axis. It was noted that the largest increase in average texture size occurred for the annealing condition of 650°C/5 s. An increase of about two orders of magnitude was observed when the film thickness increased from 100 nm to 250 nm, indicating that the average texture size for samples annealed at this condition was more responsive than all others to the change in film thickness.

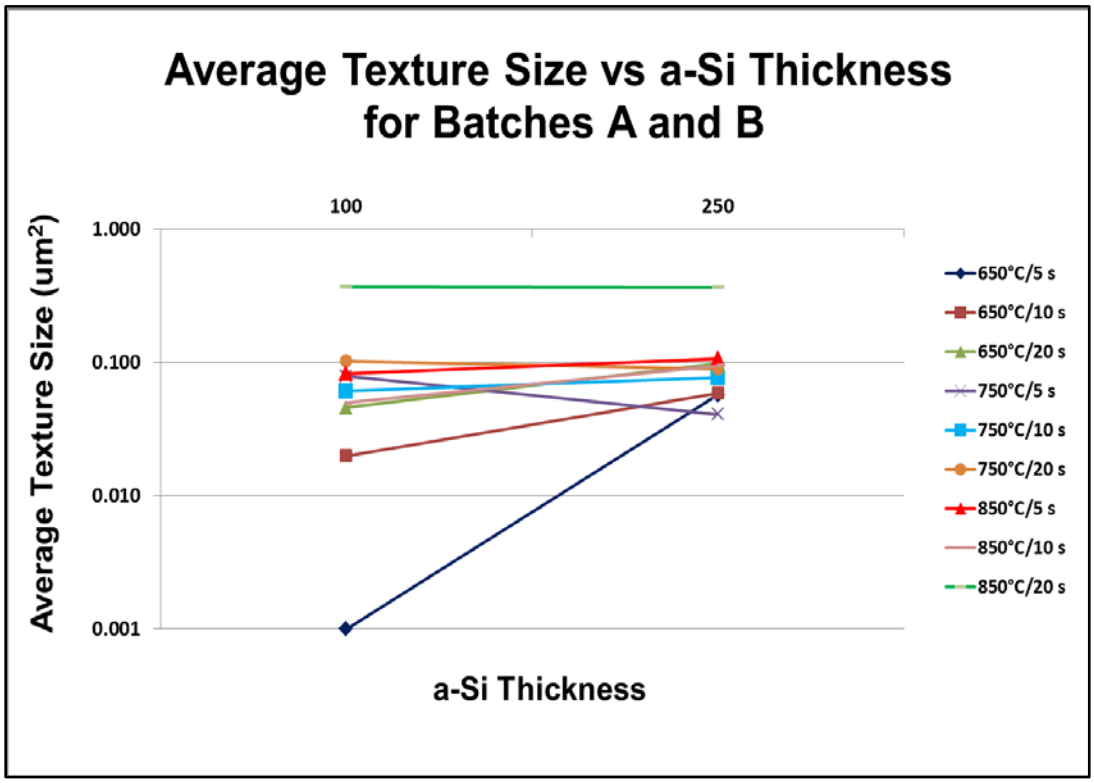

Figure 4.5. Plot of average texture size versus a-Si thickness for batches A and B.

Proceeding through the annealing conditions as presented in the legend of the figure, it was noted that the remaining durations related to the 650°C annealing temperature posted

increases in average texture size primarily because of longer annealing durations. Their order of magnitude increase was significantly less than the 650°C/5 s condition, suggesting that a limit was being approached for increasing texture size by the change in a-Si thickness alone. Supporting this observation are the tightly-clustered results obtained for the three annealing durations associated with 750°C. The trend for texture size change was essentially flat for these annealing conditions, inferring that texture size increases via an increase in a-Si film thickness had reached a saturation point.

The conditions of 850°C, for both 5 s and 10 s durations, likewise were found to not significantly affect the average texture size beyond that of the 750°C annealing conditions. However, the annealing condition of 850°C/20 s revealed a dramatic increase in average texture size. This increase, despite the change in a-Si film thickness, was attributed to annealing duration. This conclusion was affirmed by the level line connecting the results of batches A and B. So, increases in average texture size for the 850°C temperature is best achieved by changing annealing conditions, not a-Si thickness.

Particle density was affected by a-Si film thickness. The results from the comparison of particle densities of batches A and B are shown in Figure 4.6. Particle density was plotted on the vertical axis and symbolized by the number (N) of particles-per-μm^2 on the sample's surface. The horizontal axis, as before, displayed the two a-Si film thicknesses and associated data points which were identified by their annealing conditions.

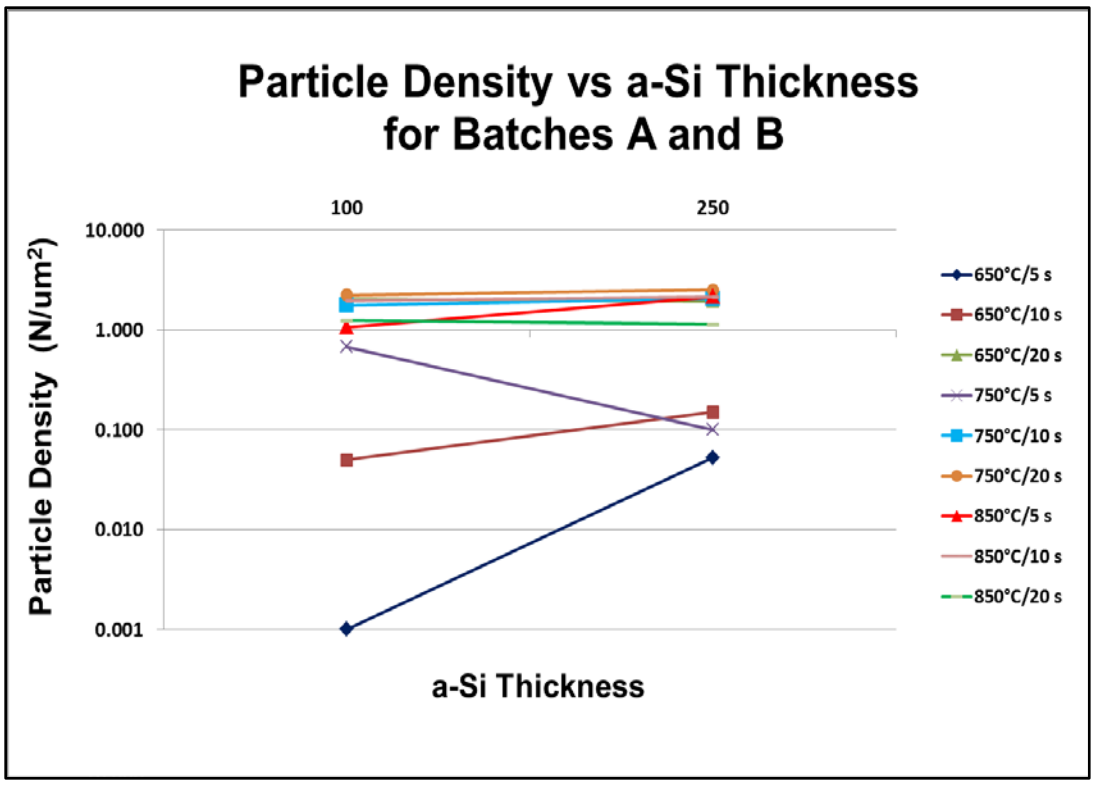

Figure 4.6. Plot of particle density versus a-Si thickness for batches A and B.

An increase in particle density approaching 2 orders in magnitude was achieved for the annealing condition of 650°C/5 s when the a-Si film thickness was increased from 100 nm to 250 nm. The a-Si thickness was most influential at this condition for changing the number of particles per-unit-area between batches A and B. The conditions of 650°C, for 10 s and 20 s, and 850°C/5 s resulted in slightly less than one order magnitude change. These conditions, however, were aided by an increase in temperature and/or duration, so they posted net increases in particle density over the 650°C/5 s condition, despite having a lower magnitude of change.

For the 750°C annealing conditions, it was observed that increases in particle density occurred as a consequence of change in annealing duration rather than a-Si film thickness. The annealing duration of 20 s produced the peak number per-unit-area of particles obtained during

nano-texture formation, but it was closely followed by the results from 10 s duration. This indicated that a saturation point for generating the highest particle count had been reached for the annealing conditions of this study. Further illustrating the importance of annealing duration were the results of the 750°C/5 s condition. Without sufficient duration to support nano-texture formation, very few textures developed. Usually, an annealing temperature increase made up for the texture deficiencies of short durations, but the 250 nm film thickness was too substantial to allow numerous texture generation at this duration.

The result of the 850°C/10 s condition also remained close to the value obtained for the peak particle count. However, for the 850°C/20 s condition, a marked increase in texture size was observed. As a consequence of texture size increase, the number of particles-per-μm^2 decreased. The decrease was the result of smaller particles coalescing into larger ones, a conclusion that the SEM images in Figure 4.3c seem to confirm.

Average particle size and particle density each play a role in affecting the percent of coverage of the samples' surface by nano-textures. Logically, the combination of the largest particle size and highest particle density would lead to the greatest amount of coverage. Figure 4.7 shows the effect of a-Si thickness on the percent of coverage. The largest particle size was created with the annealing condition of 850°C/20 s, and the results of the figure agree with this conclusion. Average particle size for this annealing condition was evidently more dominant than particle density, though not by a large degree.

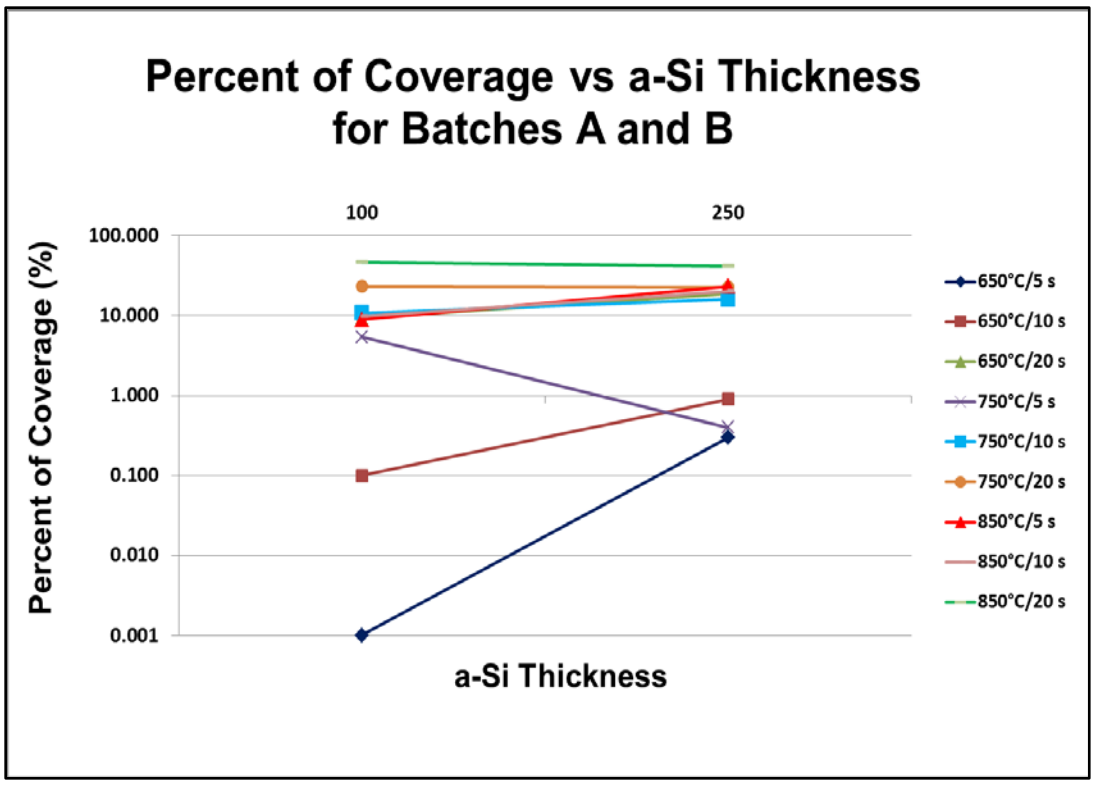

Figure 4.7. Plot of percent of coverage versus a-Si thickness for batches A and B.

Clearly, the effect of a-Si film thickness was less dominant for the 750°C and 850°C annealing conditions. Fewer sloped lines indicated this was the case. The trend of this data for percent of coverage revealed that increasing the annealing temperature and/or duration was the optimum method for improving the coverage of the surface with nano-textures. The condition of 650°C/20 s seemed to be the greatest beneficiary of the increase in percent of coverage by modifying the annealing conditions.

For the 650°C annealing conditions, there was more dependence on the increase in a-Si thickness to change the percent of coverage. The condition of 650°C/5 s demonstrated the largest change (more than 2 orders of magnitude) in surface coverage due to this effect. The condition of 650°C/10 s produced one order of magnitude in change, until finally no change due

to a-Si increase was observed for 650°C/20 s and above, suggesting once again that a saturation point in texture coverage had been achieved.

A summary of the results of Figures 4.5-4.7 is as follows. It was noticed that as a-Si thickness increased from 100 nm to 250 nm, texture size, particle density, and percent of coverage increased for the 650°C annealing condition. Increasing the a-Si thickness was the most effective way to increase these nano-texture properties. The curves of the 3 figures showed clustering and flattening trends for the 750°C annealing conditions, signifying that a saturation point in nano-texture generation had been reached by increasing a-Si thickness alone. Furthermore, it was observed that increasing the annealing duration and temperature were the most effective ways to increase texture size and percent of coverage of the surfaces for 750°C to 850°C annealing conditions. Additionally, as temperature increased from 650°C to 750°C, the particle density increased and then it decreased as the annealing temperature proceeded to 850°C, suggesting that the nano-particles were nucleating and multiplying on the surface before coalescing into larger ones, therefore yielding the decreasing particle count per-unit-area.

4.4 Study of Nano-Texturing Effect on Surface Wetting

Gaining an understanding of the relationship between a-Si film thickness, annealing conditions, and surface wetting properties was of interest to this research. Knowledge of the particular nano-texture formation conditions that most effectively produced the desired wetting behavior could, for example, benefit machinery components that require control of surface wetting for reliable operation. Two batches of nano-textured samples, labeled A and B, were tested to determine the effects of nano-texturing conditions on surface wetting. In addition, a

low surface energy film of octafluorocyclobutane (C_4F_8) was applied to a few samples to examine the ability of a chemically-modified surface to affect surface wetting.

4.4.1 Discussion and Analysis of Hydrophilic and Hydrophobic Water CA Results

Of interest was whether the samples exhibited hydrophilic or hydrophobic behavior due to nano-texturing. The water CA measurements of batches A and B samples are illustrated in Figures 4.8 and 4.9. They were obtained using a contact angle machine rather than calculations using Wenzel and Cassie-Baxter equations to avoid complications introduced by random surface orientation and sizes of particles fabricated during this study. The water CA measurements shown are values measured relative to the established standards commonly reported in literature.

The water CA results from the nine annealing conditions of batch A are plotted in Figure 4.8. Annealing conditions are displayed on the horizontal axis and water CA readings appear on the vertical axis in degrees. A visual analysis of the results shows that a range of water CA results were produced. The range spanned from hydrophilic (water CAs < 90°) to hydrophobic (water CAs > 90°). Recall that this batch was fabricated using the a-Si film thickness of 100 nm. Some unique results were obtained when an in-depth analysis was performed.

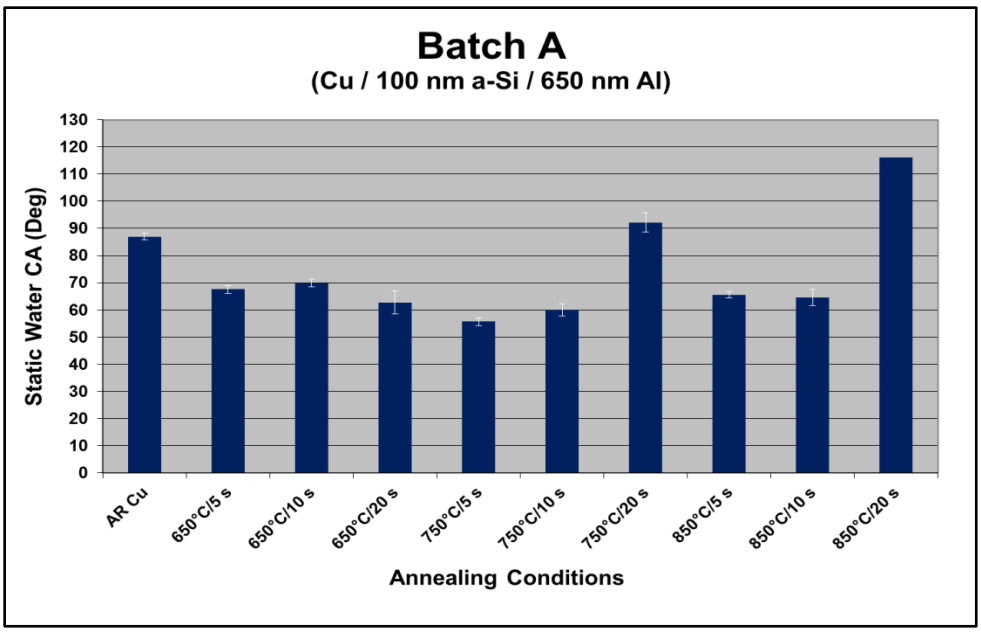

Figure 4.8. Water CA measurements taken from batch A.

AR Cu was designated the control sample in this investigation, so it became the reference surface topography for observing the effect of the AIC of a-Si nano-texturing technique applied to smooth, AR Cu substrates. The water CA measurement for AR Cu was found to be 87°, which technically made it hydrophilic, yet also very close to characterization as a neutral surface. The annealing temperature of 650°C produced a water CA of about 67° for the 3 annealing durations. These water CA results were very similar to ones obtained for a-Si film applied directly to un-textured, AR Cu substrate. An un-textured a-Si film is intrinsically hydrophilic, which explains the decrease in water CA when it was deposited on smooth Cu substrate. The 650°C/5 s annealing condition generated no discernable texture formations, so it logically resembled the 67° water CA results of a-Si film on AR Cu. However, the 10 s and 20 s durations produced nano-textures on the substrates, yet the water CAs remained close in value to that of un-textured a-Si.

The same water CA behavior was observed at 750°C, for both 5 s and 10 s annealing durations. Nano-texture formations were fabricated for these annealing conditions, but the water CA results deviated only slightly from those of the 650°C annealing conditions. Quite the opposite, the 750°C/20 s annealing condition experienced a substantial increase in its water CA measurement. A reading of 93° was achieved, representing a 30° increase over the water CAs for the other annealing conditions of 750°C. In similar fashion, the 850°C/5 s and 850°C/10 s annealing conditions yielded no appreciable difference in water CA measurements from that of AR Cu deposited with un-textured a-Si, but the 850°C/20 s annealing condition caused a huge spike in its water CA reading. For this annealing condition, a 116° water CA occurred, nearly doubling the reading of the other annealing conditions at 850°C.

A definitive pattern of water CA readings emerged from this batch of samples using 100 nm a-Si in the AIC of a-Si nano-texturing process. The water CA readings obtained from the 5 s and 10 s annealing durations, for all temperatures used in the annealing matrix, were unaffected by the presence of nano-textures. The low particle density and small texture size for these short durations failed to provide enough roughness effect to produce a meaningful change in water CA for these conditions. Apparently, though, once a nano-topography had attained an ideal nano-texture density and size, and those textures exhibited peaked formations, a spike in water CA measurement could take place. The water CAs of 750°C/20 s and 850°C/20 s annealing conditions indicated this ideal topography had occurred. The peaks sufficiently reduced the apparent CA of the water droplet resting on the nano-surface and, therefore, reduced the effectiveness of the surface's capillary action in overcoming the high surface tension of water molecules. With the smaller liquid/solid contact area, the surface forces existing on the water droplet did not have to compete as much with the energy exerted by the nano-surface and could,

consequently, permit a higher water CA reading. The peaked formations also contributed to a Cassie-Baxter mode of surface topography where the water droplet was buoyed by air pockets residing between the nano-texture and underside of the droplet, thus yielding higher water CA measurements.

The water CA measurements of batch B samples are shown in Figure 4.9. Alongside AR Cu, the nine annealing conditions are plotted on the horizontal axis, and the water CAs are shown in degrees on the vertical axis. The water CA results illustrate the effect on surface wetting when the a-Si film thickness increased from 100 nm to 250 nm. A definite trend toward lower water CAs was noticed overall for this batch as annealing temperature and duration increased. In this batch, all of the samples exhibited very hydrophilic behavior. Six of the nine annealing conditions achieved water CA readings below 20°. The highest reading of approximately 38° occurred for the annealing conditions of 650°C/5 s and 750°C/5 s. The largest water CA differential for this batch was about 30°, but it was roughly 45° for batch A.

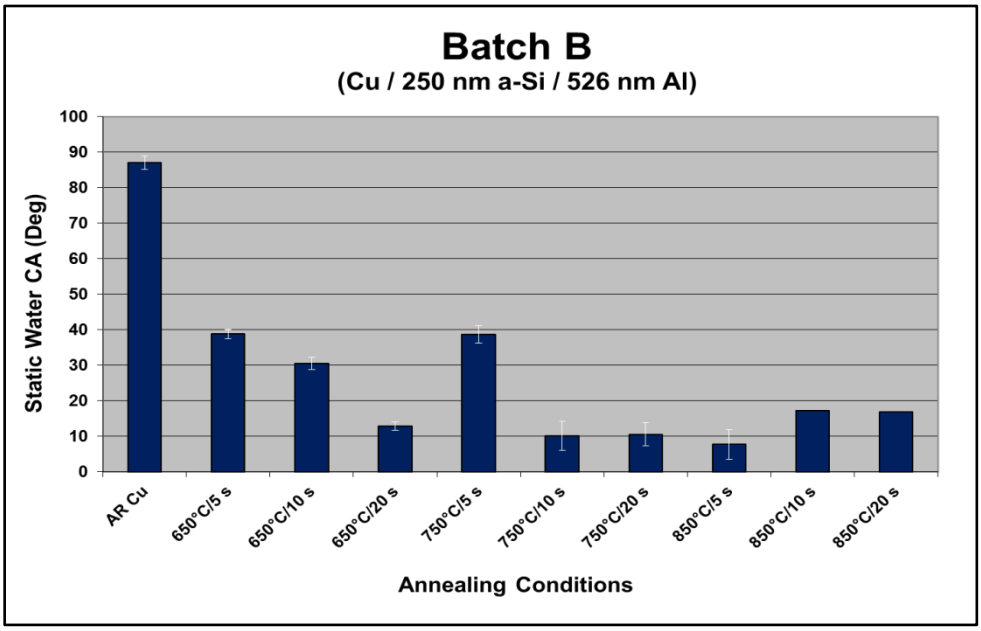

Figure 4.9. Water CA measurements taken from batch B.

For the annealing condition of 650°C/5 s, some noticeable texture formation was observed in the SEM image, whereas the same annealing condition for batch A yielded no texture. The water CA reading was inevitably lower than AR Cu due to the intrinsically hydrophilic behavior of a-Si. An increase in a-Si supply benefited nano-texture formation and produced a still lower water CA reading (approximately 38°) at the minimum annealing temperature and duration. Correspondingly, as more nano-textures formed for the annealing conditions of 650°C/10 s and 650°C/20 s, increasingly hydrophilic nano-topographies were created. As the proximity of neighboring textures increased, those textures coalesced into even larger ones, causing more hydrophilic nano-topographies to form and lower water CAs to occur.

The 750°C/5 s annealing condition did not possess the distinct crystallographic appearance of nano-textures that were formed on top of the a-Si film. The nano-topography appeared very similar to the result for 650°C/5 s annealing condition, so it was not surprising that their 38° water CA readings were identical. The annealing temperature increase at such short duration and for this film thickness was evidently insufficient to cause a perceivable difference in their nano-texture formations and water CAs. However, a significant increase in particle density and size occurred as the annealing conditions changed to 750°C/10 s and 750°C/20 s, and this resulted in about 30° of reduction in the water CAs. Both average particle size and density for these annealing conditions were nearly identical, and the similarity was reflected in their water CA readings of 11°.

Some important insights on water CA behavior can be gleaned from the formation pattern of the nano-textures created by the 650°C/5 s and 750°C/5 s annealing conditions. The appearance of the textures indicated that nucleation occurred underneath the thicker a-Si layer

before emerging on the film surface. Higher temperature and/or duration were required before manifesting the lightly-colored crystallographic structures that characterized the nano-textures of batch A. As stated earlier, the crystallization patterns tended toward lateral rather than vertical nucleation, thus making it more difficult to build increasingly taller nano-structures away from the substrate. The abundant supply of a-Si above the nucleating a-Si crystallites undoubtedly contributed to the flat-topped nano-texture formations that subsequently lowered the water CAs overall. The conclusion drawn from this observation was that the geometry of the nano-topography was an important influence in the wetting behavior of batches A and B.

Turning attention to the 850°C annealing conditions, it was observed that the 5 s duration achieved the lowest water CA reading (7°) of batch B samples. This result translated into it being the most effective annealing condition for surface wetting and it being included in the superhydrophilic regime. It should be noted that this annealing condition did not produce the largest particle size for this batch. That designation belonged to the 850°C/20 s annealing condition. But, the 850°C/5 s annealing condition did post one of the highest particle densities in conjunction with a large particle size, and these traits distinguished the annealing condition for its superior wetting performance. On the other hand, the 850°C/10 s and 850°C/20 s annealing conditions caused an increase in water CA readings, rising to approximately 17°. Especially for 850°C/20 s was the increase in particle size and percent of coverage of surface significant. Evidently, there existed a particle size and surface coverage limitation for decreasing the water CA at this annealing condition. The nano-texture coverage, in effect, began to cause the surface to resemble a continuous a-Si film which produced a higher water CA measurement.

Interesting contrasts between the water CAs of the batches existed and were useful in selecting the textured samples chosen for further testing. As Figure 4.10 demonstrates, both

batches produced abundant hydrophilic samples which could provide opportunities to test improvement in lubricant retention and friction reduction using nano-textured surfaces. Two sample conditions, 750°C/20 s and 850°C/5 s, achieved extraordinary water CA measurements of 10° and 7°, respectively. They were chosen, along with an AR Cu sample, to proceed to oil CA characterization and dry friction testing.

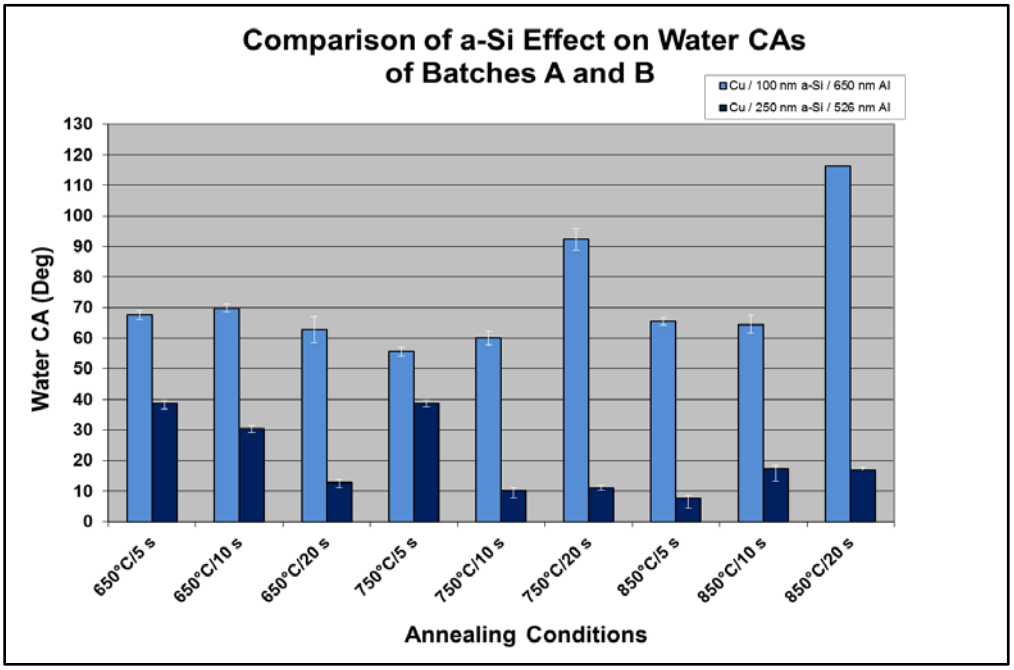

Figure 4.10. Water CA comparison used to select the samples for oil CA and friction testing.

Since non-wetting of material surfaces was a topic of great interest in nano-surface engineering, attention was given to the creation of superhydrophobic nano-topographies on Cu substrate. Using select annealing conditions from batch B samples, hydrophilic nano-topographies were generated. In Figure 4.11, water CA measurements for a few textured samples (in particular, those having water CAs less than 20°) were plotted, and the results demonstrated the benefits of modifying the surface chemistry to transform superhydrophilic

nano-textured surfaces to superhydrophobic ones. Nano-textured surfaces were fabricated using AIC of a-Si in order to generate the roughness necessary to achieve superhydrophilicity and superhydrophobicity. To reduce the intrinsically hydrophilic effect of a-Si film, a 20 nm thick, low surface energy film of C_4F_8 was applied over the nano-topography using a modified deep reactive ion etching (DRIE) process. Doing so permitted the roughness of the nano-textures to be used to maximum effect for creating a Cassie-Baxter condition of surface wetting and achieve very hydrophobic and superhydrophobic nano-topographies.

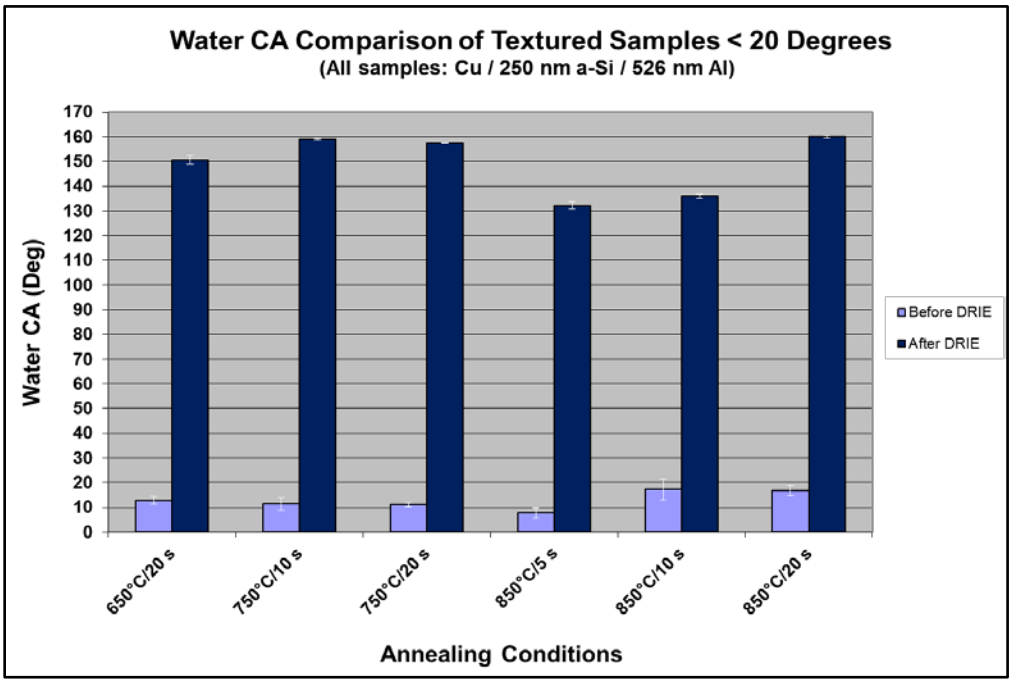

Figure 4.11. Water CAs of nano-topographies before and after DRIE.

The results of DRIE and its effect on water CA readings were mixed. Ideally, the lowest water CA, which was incidental to the highest surface roughness, should have produced the highest water CA when C_4F_8 was applied. The 850°C/5 s annealing condition was the most hydrophilic water CA at 7°, yet the reading after DRIE was only 132°. No coherent explanation

can be offered, except that perhaps the C_4F_8 coverage was insufficient, therefore allowing the hydrophilic nature of a-Si to affect the water CA result. Also possible was some diminishing effect on the water CA readings due to geometric properties of the broader, and less peaked nano-textures that were generated by the thicker a-Si film. These same reasons might explain the 134° water CA result of the 850°C/10 s annealing condition.

Despite the anomalies mentioned above, the other annealing conditions produced a number of opportunities for creation of nano-topographies having water CAs greater than 150° after the application of C_4F_8. The 650°C/20 s annealing condition was the minimum test condition to achieve superhydrophobicity. Two annealing conditions for 750°C generated superhydrophobic surface wetting results: 750°C/10 s and 750°C/20 s. Their water CA readings were 159° and 158°, respectively. The highest water CA was achieved by the 850°C/20 s annealing condition, which was 161°. It appears that a correlation existed between the hydrophobicity of the nano-surfaces that achieved water CAs greater than 150° and the percent of coverage of surface. For example, the 850°C/20 s annealing condition featured the highest percent of coverage, and it correspondingly attained the highest water CA of 161°. The 750°C/10 s and 750°C/20 s annealing conditions were tied second for highest coverage and hydrophobicity (water CAs of about 158°).

4.4.2 Static Oil CA Results of Amphiphilic Nano-Topographies

No literature could be found that discussed using nano-topographies on Cu as lubricant retainers. The surface wetting results obtained with water were encouraging enough to explore the possibility of using nano-textures to promote surface wetting using a hydrocarbon such as mineral oil. If successful, applications that required lubricant replenishment and retention could

benefit tremendously from nano-topographies that have amphiphilic properties. An amphiphilic surface is one that has an affinity for both water and oil, although not simultaneously. This type of nano-surface could be primed with either fluid of interest and be expected to perform its function of surface wetting quite effectively.

A rationale was established for selecting the annealing conditions and resulting nano-topographies to undergo static oil retention testing. From Figure 4.10, the annealing conditions of 750°C/20 s and 850°C/5 s were chosen, not only because they were the most hydrophilic and therefore the most likely to succeed for oil retention, but also for the reason that they exhibited excellent adhesion of their nano-topographies to the substrate. Concerns about the chemical interaction of the lubricant with the a-Si film and the physical preservation of the nano-topography after the oil was deposited on the surface were issues which had to be confronted, too. After lubrication, some of the samples were spin-tested at 7200 rpm and duration of 105 s using a spin coater. This process removed a significant portion of the 40 mg of oil that was deposited on the nano-topographies. An inspection of the SEM images of the lubricated and spun samples found that the nano-textures remained intact, thus nullifying concerns regarding the survival of nano-textures in a hydrocarbon environment.

Oil droplets having a volume of 3 μL were dispensed on the AR Cu and nano-topographies for static oil CA measurements. The purpose of the measurements was to investigate whether nano-textured surfaces could serve as a reservoir to retain lubricant. The graph in Figure 4.12 shows the results. The control sample, AR Cu, with an oil CA of 29°, had the highest CA of the sample types tested. It proved to be oleophilic, or possessing an affinity for oil, although not entirely from its intrinsic surface energy. The relative surface energy of AR Cu was not high, as indicated by the 87° water CA. AR Cu retained a lubricant on its surface

from the viscous and polar effects of the oil, as well as from the presence of surface micro-pits and polishing grooves created during the mirror-finishing of its surface. These surface features are shown in Figure 4.13.

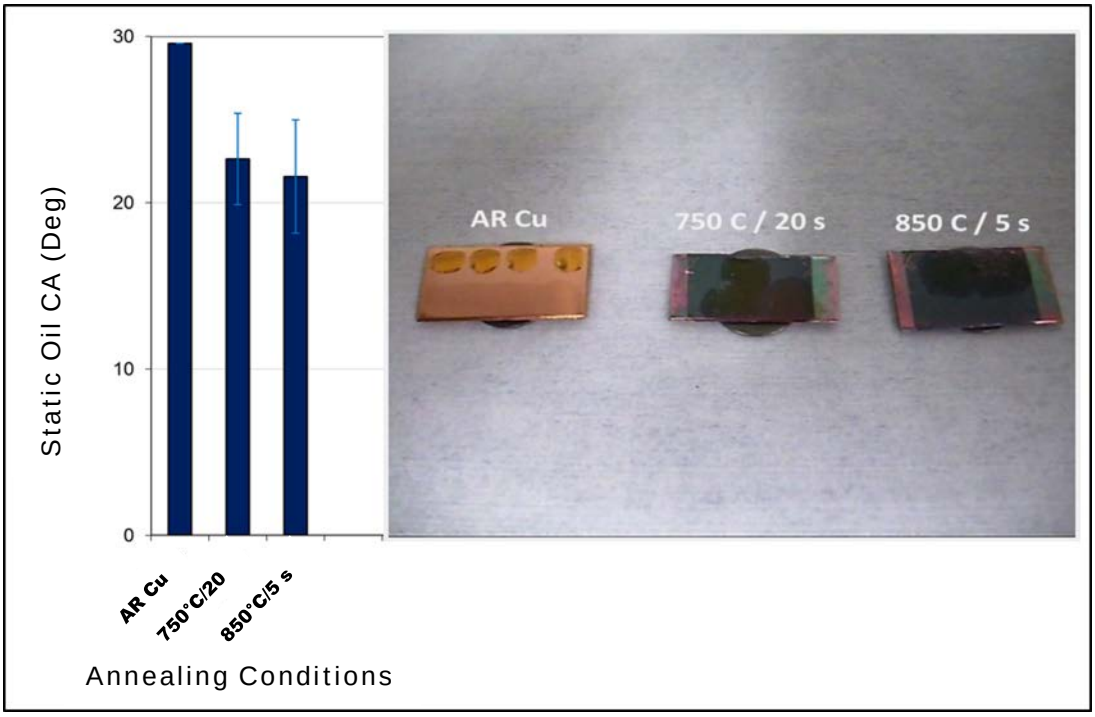

Figure 4.12. Plot of oil CA tests and photograph of oil retention results of AR Cu and nano-textured surfaces.

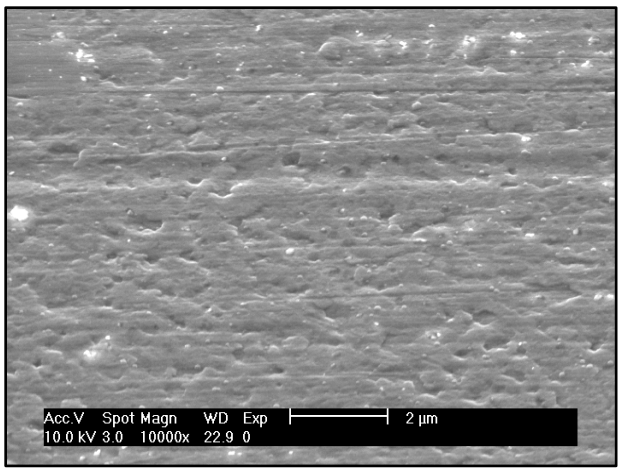

Figure 4.13. An SEM image of AR Cu surface featuring micro-pits, grooves, and polishing lines that served as lubricant retainers. The image was captured at 10k magnification.

Profilometry measurements revealed that the groove depths were approximately 72 nm. The pits and grooves served effectively as lubricant reservoirs. A tilted surface or induced dynamic condition, however, changed the ability of the surface to retain a constant volume of lubricant without replenishment. The droplets shown on the AR Cu surface in Figure 4.12 eventually migrated toward one another while resting on a slightly irregular surface, proving that the minimum dynamic force could displace lubricant from an un-textured Cu surface very easily.

A different result occurred on the nano-textured samples fabricated by the 750°C/20 s and 850°C/5 s annealing conditions. The oil CA measurements for those samples were 23° and 21°, respectively, thus demonstrating an immediate improvement in oleophilicity over AR Cu. Figure 4.12 shows the results of placing three 3-µL oil droplets on each nano-topography and the subsequent wetting behavior. It should be noted that the ends of the nano-textured samples, a total area measuring about 6 mm x 13 mm, were not processed using the AIC of a-Si technique. During nano-texturing, these ends were used for securing the samples by placing polyimide tape across them. A clear demarcation line between the textured and un-textured portions was

confirmed by the abrupt stop in the oil spreading pattern on each sample as the oil reached the unprocessed portions.

Unlike the standing droplets on the AR Cu sample, the nano-textured samples readily absorbed the 7.2 mg of oil in the nano-textures within a few minutes. Two mechanisms contributed to the increased adsorption of oil on Cu substrate. The first was the increased oleophilicity due to a-Si having amphiphilic properties. This property was responsible for the spreading of the oil along the nano-topography. The second was the creation of voids or valleys between the peaks of the nano-textures that served as reservoirs for the oil. The void volume created during the nano-texturing process was obviously superior to the micro-features of AR Cu by noting that all of the oil was absorbed into the nano-voids. Even tilting the samples vertically failed to displace the lubricant from the nano-surfaces. Of course, the nano-surfaces could be saturated to the point of excess, and this condition would lead to oil run-off. The maximum volume of oil retained or the porosity of particular nano-topographies will be an area of future study. Nonetheless, it was established that nano-textures can serve as a reservoir for lubricants.

4.5 Investigation of Nano-Texturing Effect on COF

An important application of nano-texturing is to reduce friction as two contacting surfaces move relative to the other. Ideally, nano-textures reduce the amount of projected surface contact between specimens, therefore lowering the friction. The nano-sized asperities could permit shearing and rolling of the peaks and an increase in plasticity or plowing of the nano-material as the surfaces slid, thus behaving similar to the effect of lubrication [75-78]. Three samples were tested: AR Cu and nano-topographies fabricated via 750°C/20 s and

850°C/5 s annealing conditions. Tests were performed on the samples under different normal loads to generate plots of the COF as a function of normal load.

The COF result of one of the loading conditions is illustrated in Figure 4.14. Shown in the figure is the COF produced on an AR Cu sample as a function of time. The COF measurement was plotted on the vertical axis of the graph and defined as the lateral force (LF) divided by the normal force (NF). A 7000 μN normal force was applied to the AR Cu sample to achieve this result. The curve illustrated the interfaces' frictional behavior as the normal force was applied to the TriboIndenter's tip as it slid across the surface.

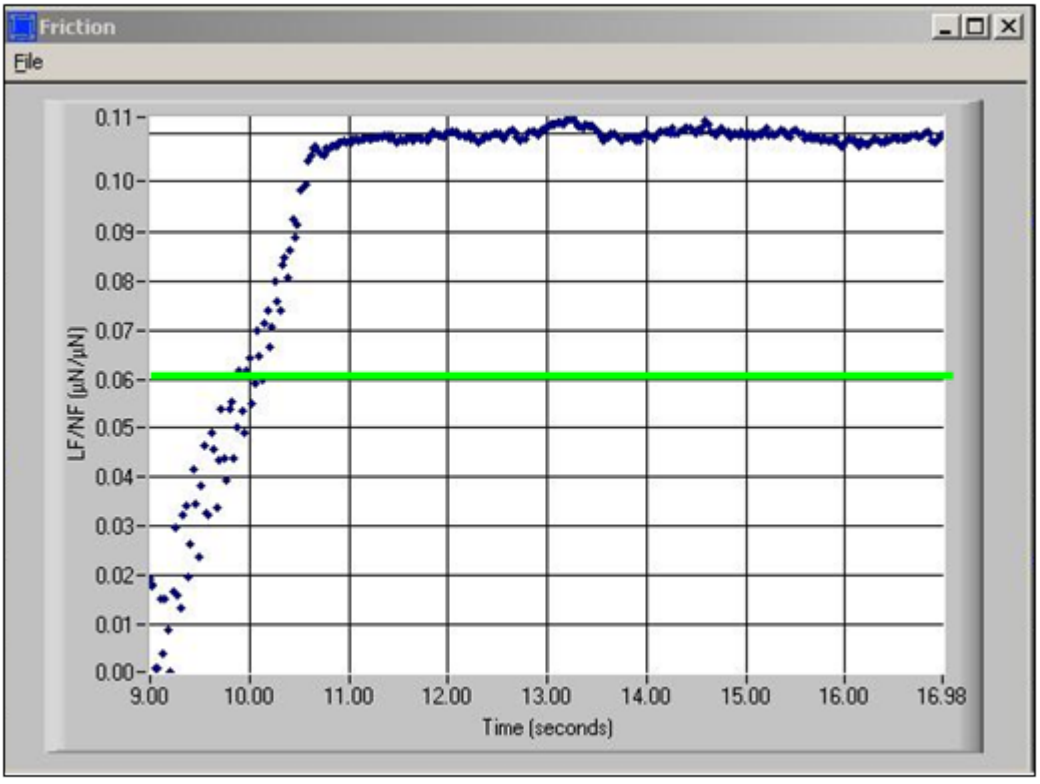

Figure 4.14. COF analysis of the AR Cu sample was performed on the Hysitron TriboIndenter.

The curve shows that between 9 s to 10.5 s, the tip is in static contact with the sample and the relative motion starts at 10.5 s when the kinetic friction takes place. It was observed that the maximum static and kinetic COF values were similar. A number of factors had an effect on the COF. The surface of Cu is very soft and some material yielding might have occurred as the relatively small, 100-μm radius tip was pushed into the substrate. Another factor affecting the COF result was the tilt of the surface relative to the tip. The surfaces of the AR Cu samples were not perfectly flat after fabricating them from a larger sheet of metal, so some variation in the COF readings was expected as the applied normal force was affected by a tangential component of force imposed by the non-uniform surface. As a result, the tip experienced some sticking behavior during the scratch test.

The region of the graph between 10.5 s and 17 s shows small variations in the kinetic COF which could be caused by surface plowing. The measured COF is 0.1 ± 0.005 for AR Cu after averaging the data for 5 scratches. This is the result plotted at the 7000 μN normal force position on the AR Cu graph in Figure 4.15. For comparison, the green line shown on Figure 4.14 represents the lowest COF obtained by the nano-topographies, therefore confirming that nano-textures helped to reduce friction.

Dry friction testing occurred over a wide load range on the 3 samples using the Hysitron TriboIndenter, and the results are plotted in Figure 4.15. The tested normal loads of 50, 100, 200, 300, 600, 1000, 2000, 3000, 5000, 7000, and 10,000 μN are shown on the horizontal axis. The load values were chosen to take advantage of the TriboIndenter's full load range and to facilitate a smoother plot of COF. Most of the loads were multiples of each other which allowed convenient comparisons of friction results and observation of distinctive behavioral patterns.

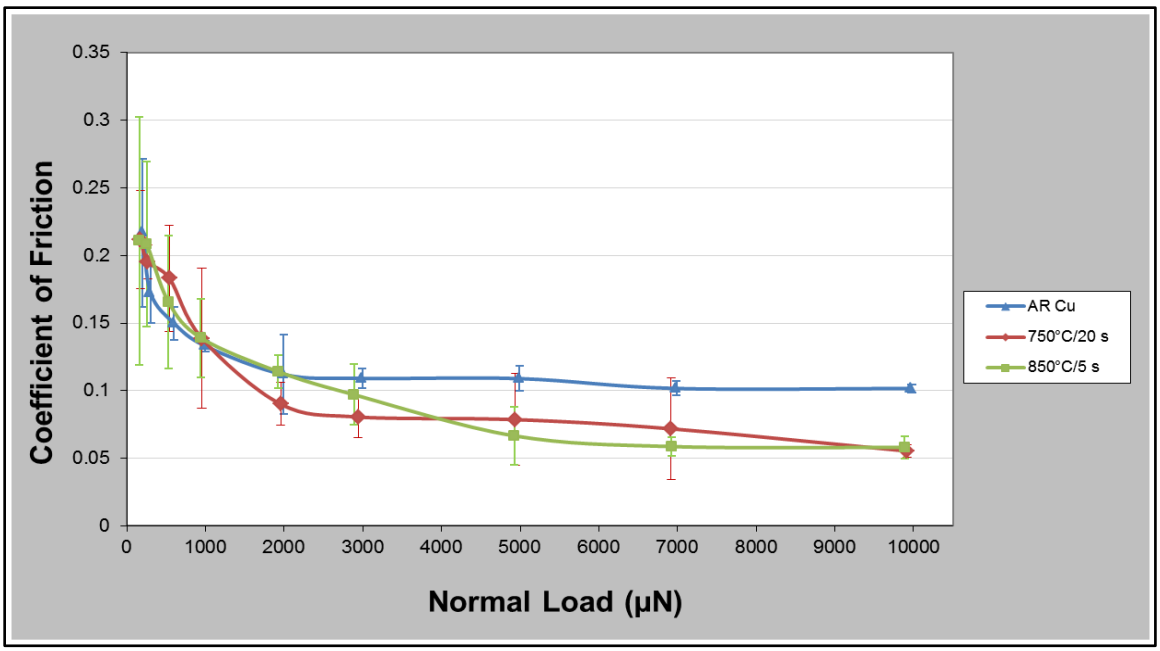

Figure 4.15. Plot of coefficient of friction versus normal load for AR and nano-textured Cu. The maximum reduction in COF was 40 percent at 10,000 µN normal load.

The COF for AR Cu began around 0.22 for normal loads under 200 µN and dropped to about half that value, 0.12, by the 2000 µN load test. The COF held a consistent value of about 0.12 between the 2000 µN and 5000 µN load range, and subsequently reduced to its lowest value of 0.1 starting from 7000 µN. At small normal loads, adhesion force is comparable to or more than the normal force which leads to higher friction force. However, since the adhesion force is not used in the COF calculation, the calculated COF is higher due to increased lateral force caused by adhesion force. As the normal force increases, the adhesion forces' contribution to COF decreases, which explains the dramatic decrease in COF that happened at normal loads higher than 200 µN.

At the micro- and nano-scale, adhesion and plastic deformation both contribute to friction force [3]. The purpose of nano-texturing was to reduce the area of contact and therefore lower the adhesion component of friction force. The lower COF of the nano-topographies was the

result of the smaller area of contact between the tip and the nano-textured surface compared to the area of contact between the tip and smooth AR Cu surface. Also, as the normal load increased, the contribution of the adhesion component to the friction force decreased, in turn causing the COF to decrease [43].

Nano-texturing on Cu produced no tangible benefit for loads under 1000 μN; in fact, the COF was shown to increase slightly for both nano-topographies in this region. However, the variation of COF was very large for the 3 samples, indicating that the difference between the COF of AR Cu and the nano-textured samples may not be significant. It is not known whether debris from individual nano-textures dislodged and affected the ability of the tip to accurately sense the nano-surfaces at low normal loads. However, as the normal loads increased, the presence of debris would not be a concern because it could be easily compressed.

The nano-textured samples exhibited COF values below that of AR Cu, starting around the 2000 μN normal load. The nano-topography fabricated from the 750°C/20 s annealing condition achieved a three-fold decrease in COF from the 50 μN to 3000 μN normal loads. The COF remained constant at 0.08 for 3000 μN to 5000 μN normal loads, indicating plastic deformation was the main mechanism of friction. Increasing the normal load caused the COF to decrease linearly from 0.08 to 0.06, beginning at the 5000 μN load and continuing through the remainder of the tests.

The 850°C/5 s annealing condition registered the largest continuous change in COF by achieving a decrease from 0.22 to 0.07 from 50 μN to 5000 μN loads. The reduction of adhesion due to nano-texturing and increasing the normal loads contributed to the COF reduction in this region. The COF behavior was smoother and more predictable, as observed by the gently sloping curve of this plot versus the abrupt change of the others. Only a minor COF decrease

occurred during the 5000 µN to 10000 µN load range, making this nano-topography the more stable of the two tested under high loads.

The plots of the COF of the nano-textured surfaces relative to each other were interesting, especially between the 1000 µN and 4000 µN, and 4000 µN and 10,000 µN load tests. The differences in COF were as much as 0.05. Since the average particle size, particle density, and percent of coverage of the nano-topographies were nearly identical, the reasons for the COF differences are presently not understood. It is surmised that subtle differences in the nano-topographies were responsible in some way for the variations in COF. At the 10,000 µN load test, the nano-textured surfaces of the 750°C/20 s and 850°C/5 s annealing conditions achieved 0.06 COF measurements for a maximum reduction in friction of 40 percent.

CHAPTER 5

CONCLUSIONS AND FUTURE WORK

5.1 Conclusions

The AIC of a-Si process was used to fabricate various nano-topographies on Cu substrate to study surface wettability and COF. An investigation of the effects of changing annealing conditions and a-Si thickness was performed to examine their impact on nano-texture formation. Samples in batch A were deposited with 100 nm thick a-Si and batch B received 250 nm. To create the different nano-topographies, the annealing temperature and duration of both batches were modified according to an annealing matrix that featured temperatures of 650°C, 750°C, and 850°C and durations of 5 s, 10 s, and 20 s for each of these temperatures. SEM images of the nano-topographies were obtained for qualitative and quantitative analysis of the nano-topographies to determine correlations between the batches' texture size, density, percent of coverage, and surface wetting. Chemical modification of the surfaces of select samples of batch B was performed to demonstrate the conversion of hydrophilic nano-topographies to superhydrophobic ones. Also, COF testing of AR Cu and nano-topographies was performed for assessing whether nano-textured surfaces could provide friction reduction below AR Cu substrate.

There were similarities between the batches that were noteworthy. Generally, as the annealing temperature increased, the nano-texture formations increased in size, density, and percent of coverage on the surface. The same was true for annealing duration; that is, the formations also increased in size, density, and percent of coverage as the duration increased.

Aside from these similarities, the differences were revealing for nano-texture formation. For example, it was noticed on the graphs of a-Si effects that when the a-Si thickness increased from 100 nm to 250 nm, texture size, particle density, and percent of coverage of the surfaces increased for the 650°C annealing conditions. This indicated that increasing the a-Si thickness was the most effective way to increase these properties at this temperature. The clustering and leveling trends observed on the graphs for the 750°C annealing conditions implied that a saturation point in nano-texture formation had been reached by increasing a-Si thickness only.

Additionally, it was observed that increasing the annealing duration was the most effective way to increase texture size and percent of coverage of the surfaces for the 750°C and 850°C annealing conditions. Furthermore, as temperature increased from 650°C to 750°C, the particle density increased, but then it decreased as the annealing temperature proceeded to 850°C, suggesting that smaller nano-particles were proliferating on the surface before coalescing into larger ones, therefore yielding a decreasing particle count per-unit-area.

The surface wetting results correlated very well with the nano-topographies that were created by the annealing conditions and a-Si thickness change. In general, as the annealing temperature and/or duration increased and more nano-textures formed on the substrates, the water CA readings tended to decrease. Surface nanoscale roughness was undoubtedly a factor, but the geometries of the nano-textures of the batches were important in the results, too. Two dominant particle geometries emerged in response to the a-Si thickness change: batch A produced smaller, spiked texture formations and batch B produced larger, and less peaked ones as expected from the thicker a-Si layer. For batch A, the small, spiked formations did not affect water CA results significantly until certain particle density and size combinations were reached.

This was the reason for the two hydrophobic spikes in water CA readings in otherwise stable results.

Batch B water CA results were the most responsive to change in annealing conditions and a-Si thickness. Having a greater a-Si supply was instrumental in creating all-hydrophilic nano-topographies, of which six had water CAs less than 20°. Two of the topographies produced superhydrophilic results, due to the high particle count and large texture size combinations they possessed. When the surfaces of six different nano-topographies from this batch were deposited with the low surface energy film of C_4F_8, four of them became superhydrophobic. The ones that did not were likely affected by insufficient C_4F_8 coverage or texture geometry issues.

Also investigated was the possibility of using nano-topographies as lubricant retainers. Oleophobic and oleophilic nano-topographies had been produced on other metal substrates, but no research had used a nano-topography on Cu for these purposes. AR Cu and two nano-textured samples were tested to determine if nano-texures improved the surface's affinity for oil. It was found that the textures were oleophilic, as proven by the spreading of oil along the nano-topography due to the capillary action of crystallized a-Si. The oil CAs of the nano-textured surfaces was lower, indicating that they had higher oil affinity than AR Cu.

The SEM images of AR Cu revealed that its surface contained micro-pits and grooves that helped it to retain lubricants. However, the retention of the nano-textured surfaces was superior to AR Cu because the higher void volume of the nano-topographies absorbed the oil between the textures readily. Clearly, the nano-topographies could have held more oil than shown. Testing of the nano-topographies' potential for dynamic oil retention and nano-surface porosity studies will be undertaken in the future.

Finally, the nano-textured surfaces were tested for COF using a TriboIndenter. The TriboIndenter applied eleven normal loads ranging from 50μN to 10,000 μN on AR Cu and nano-textured samples. The lateral force was measured simultaneously as the tip was dragged across the surfaces. The nano-textured surface decreased the contact area of the tip, therefore providing lower friction force and COF. The results of the COF for nano-topographies varied only slightly from AR Cu under low loads, but the nano-topographies quickly distinguished themselves as superior friction reducers as the normal loads proceeded higher. Overall, the nano-textured surfaces achieved a 40% reduction in COF.

5.2 Future Work

Common problems which hasten machinery component failures are excessive friction and overheating due to loss of lubrication. The random, unpredictable nature of these failures is cause for serious concern because they are directly linked to product durability and the profitability of suppliers and customers. The unpredictability of these failures can be illustrated by considering an example: while mechanical face seals last typically about 15000 h when used in domestic water pumps under continuous service, they may last only 2000-8000 h in industrial applications, to as little as a few minutes when used as a cryogenic liquid seal in a rocket engine turbopump [79]. Mechanical seal failures could also lead to catastrophic equipment failures which could cause plant shut-downs, leading to increased production and product costs [80].

Seals, bearings, and other contacting components could benefit from hydrophilic/oleophilic or amphiphilic surfaces. Nano-engineered textures using AIC of a-Si can significantly improve the amphiphilic properties of a surface, making it possible for them to retain fluids such as water and oil. Use of nano-engineered textures for friction and wear

reduction could extend component and lubricant life by lowering the overall operating temperature.

An in-depth study of the optimum amphiphilic surface wetting properties of nano-topographies to facilitate the maximum retention of lubricants is vital to enhancing mechanical face seal durability. Future directions in mechanical face seal research related to AIC of a-Si includes: (1) understanding and controlling the AIC of a-Si process to produce nano-engineered mechanical seal surfaces with optimal nano-topographies, (2) understanding how surface nano-topography affects amphiphilic wetting properties, and (3) evaluating the effects of surface micro- and nano-texturing on lubricant retention, hydrodynamic effect generation, wear and friction reductions of the mechanical seals, and the overall seal performance.

Alternative approaches to the traditional use of the AIC of a-Si technique will be considered. Sandblasting on Cu has been demonstrated to produce micro-textured surfaces on Cu substrate [53]. AIC of a-Si alone has been used successfully to produce hydrophilic and hydrophobic nano-textured surfaces on Cu substrates. When AIC of a-Si is combined with sandblasting to generate micro- and nano-asperities, the two methods have potential to enhance the tribological properties of machinery components. AIC of a-Si combined with sandblasting Cu is a micro/nano-texturing method to be explored to generate amphiphilic surfaces on mechanical face seals.

REFERENCES

1. Burton, Z., and Bhushan, B., "Hydrophobicity, Adhesion, and Friction Properties of Nanopatterned Polymers and Scale Dependence for Micro- and Nano-electromechanical Systems", *Nano Letters*, Vol. 5, No. 8 1607-1613, 2005.

2. Komvopoulos, K., "Adhesion and Friction Forces in Microelectromechanical Systems: Mechanisms, Measurement, Surface Modification Techniques, and Adhesion Theory", *Journal of Adhesion Science and Technology*, Vol. 17, No. 4, pp. 477-517, 2003.

3. Yoona, E.-S., et al., "Tribological Properties of Bio-Mimetic Nano-Patterned Polymeric Surfaces on Silicon Wafer", *Tribology Letters*, Vol. 21, No. 1, 2006.

4. Jung, Y., and Bhushan, B., "Contact Angle, Adhesion, and Friction Properties of Micro- and Nano-Patterned Polymers for Superhydrophobicity", *Nanotechnology*, Vol. 17, pp. 4970–4980, 2006.

5. Taolei, S., et al., "Bioinspired Surfaces with Special Wettability", *American Chemical Society*, Vol. 38, No. 8, pp. 644-652, 2005.

6. Koo, J., *Polymer Nanocomposites, Processing, Characterization, and Applications*, McGraw-Hill, 2006.

7. Kelly, K., et al., "The Optical Properties of Metal Nanoparticles: The Influence of Size, Shape, and Dielectric Environment", *Journal of Physical Chemistry B*, Vol. 107**,** pp. 668-677, 2003.

8. Fecht, H. and Werner, M., *The Nano-Micro Interface—Bridging the Micro and Nano Worlds*, Wiley-VCH, 2004.

9. Yu, Y., et al., "Gold Nanorods: Electrochemical Synthesis and Optical Properties", *Journal of Physical Chemistry B*, Vol. 101, No. 34, pp. 6661–6664, 1997.

10. Link, S., and El-Sayed, M., "Spectral Properties and Relaxation Dynamics of Surface Plasmon Electronic Oscillations in Gold and Silver Nanodots and Nanorods", *Journal of Physical Chemistry B*, Vol. 103, No. 40, pp. 8410-8426, 1999.

11. Hao, E., et al., "Synthesis and Optical Properties of "Branched" Gold Nanocrystals", *Nano Letters*, Vol. 4, pp. 327-330, 2004.

12. Wenzel, R., "Resistance of Solid Surfaces to Wetting by Water", *Industrial and Engineering Chemistry*,Vol. 28, No. 988, pp. 7426–7431, 1936.

13. Cassie, A., and Baxter, A., "Wettability of Porous Surfaces", *Transactions Faraday Society*, Vol. 40, pp. 546-551, 1944.

14. Erbil, H., and Cansoy, C., "Range of Applicability of the Wenzel and Cassie-Baxter Equations for Superhydrophobic Surfaces", *American Chemical Society*, Vol. 25, No. 24, pp. 14135-14145, 2009.

15. Hao, E., Zou, S., and Schatz, G., "Nanoparticles and Nanowire Building Blocks—Synthesis, Processing, Characterization, and Theory", *Materials Research Society Symposium Proceedings*, Vol. 818, p. 53, 2004.

16. Yoon, T-S., et al., "Monolayer Formation of Colloidal Nanoparticles on Various Substrates by Single and Multiple Dip-Coating Process", *Materials Science Forum*, Vols. 475-479, pp. 3811-3814, 2005.

17. Yoon, T-K, et al., "Single and Multiple-Step Dip-Coating of Colloidal Maghemite (g-Fe_2O_3) Nanoparticles onto Si, Si_3N_4, and SiO_2 Substrates", *Advanced Functional Materials*, Vol. 14, No. 11, pp. 1062-1068, 2004.

18. Klein, R., et al., "Producing Super-Hydrophobic Surfaces with Nano-Silica Spheres", *Zeitschrift fuer Metallkunde/Materials Research and Advanced Techniques*, Vol. 94, No. 4, pp. 377-380, 2003.

19. Hong, Y., et al., "Controlled Two-dimensional Distribution of Nanoparticles by Spin-Coating Method", *Applied Physics Letters*, Vol. 80, No. 5, p. 844, 2002.

20. Liu, F., et al., "Rapid Fabrication of High Quality Self-Assembled Nanometer Gold Particle by Spin Coating Method", *Microelectronic Engineering*, Vol. 67-68, pp. 702-709, 2003.

21. Singh, D., Singh, A., and Srivastava, O., "Formation and Size Dependence of Germanium Nanoparticles at Different Helium Pressures", *Journal of Nanoscience and Nanotechnology*, Vol. 3, No. 6, pp. 545-548, 2003.

22. Hrbek, J., "Growth of Metal and Metal Compound Nanoparticles on Surfaces", *Abstracts of Papers, 229th ACS National Meeting, San Diego, CA, United States, March 13-17, 2005*.

23. Zhou, L., et al., "Nanometer Scale Island-Type Texture with Controllable Height and Area Ratio formed by Ion-Beam Etching on Hard-Disk Head Sliders", *Nanotechnology*, Vol.10, No. 4, pp. 363-372,1999.

24. He, W., et al., "Micro/Nano Machining of Polymeric Substrates by Ion Beam Techniques", *Microelectronic Engineering*, Vol. 65, No. 1-2, pp. 153-161, 2002.

25. Di, F., et al., "Nano-Optical Elements Fabricated by E-beam and X-ray Lithography", *Proceedings of SPIE-The International Society for Optical Engineering, 5225 (Nano- and Micro-Optics for Information Systems)*, pp. 113-125, 2003.

26. Asakawa, K., and Ishizuka, M., “Nano-Photonic Technologies: Photonic Crystals and Quantum Dots”, *Optronics*, Vol. 244, pp. 139-144, 2002.

27. Murillo, R., et al., “Fabrication of Patterned Magnetic Nanodots by Laser Interference Lithography”, *Microelectronic Engineering*, Vol. 78-79, pp. 260-265, 2005.

28. Kono, Y., et al., “Study on Nano Imprint Lithography by the Pre-exposure Process (PEP)”, *Proceedings of SPIE-The International Society for Optical Engineering, 5753 (Pt. 1, Advances in Resist Technology and Processing XXII)*, pp. 912-925, 2005.

29. Choi, D-G., et al., “Two-Dimensional Polymer Nanopattern by Using Particle-Assisted Soft Lithography”, *Chemistry of Materials*, Vol. 16, No. 18, pp. 3410-3413, 2004.

30. Roach, P., Shirtcliffe, N., and Newton, M., “Progress in Superhydrophobic Surface Development”, *Soft Matter*, p. 4, 232-3, 2008.

31. Wang, D., et al., “Engineering a Titanium Surface with Controllable Oleophobicity and Switchable Oil Adhesion”, *Journal of Physical Chemistry*, Vol. 114, pp. 9938-9944, 2010.

32. Petzow, G., *Metallographic Etching-Metallographic and Ceramographic Methods for Revealing Microstructure*, American Society for Metals, 1976.

33. Gall, S., et al., “Aluminum-Induced Crystallization of Amorphous Silicon”, *Journal of Non-Crystalline Solids*, Vol. 299-302, pt. B, pp. 741-745, 2002.

34. Gall, S., et al., “Polycrystalline Silicon on Glass by Aluminum-Induced Crystallization”, *Conference Record of the Twenty-Ninth IEEE Photovoltaic Specialists Conference 2002 (Cat. No.02CH37361)*, pp. 1202-1205, 2002.

35. Cheng, C., Leung, T., and Poon, M., “The Effect of Nickel Seed Position on Nickel-Induced-Lateral-Crystallization of Amorphous Silicon”, *Proceedings of the IEEE Hong Kong Electron Devices Meeting*, pp. 97-100, 2001.

36. Khalifa, F., *Analysis of Aluminum Enhanced Crystallization of Hydrogenated Amorphous Silicon at Low Temperatures*, University of Arkansas, 1999.

37. Nast, O., et al., “Aluminum-Induced Crystallization of Silicon on Glass for Thin Film Solar Cells”, *Solar Energy Materials and Solar Cells*, Vol. 65, No. 1, pp. 385-392, 2001.

38. Zou, M., et al, “Nano-Aluminum-Induced Low-Temperature Crystallization of PECVD Amorphous Silicon”, *Electrochemical and Solid-State Letters*, Vol. 8, No. 7, pp. G179-G181, 2005.

39. Zou, M., Cai, L., and Wang, H., "Nano-Aluminum-Induced Crystallization of Amorphous Silicon”, *Materials Letters*, Vol. 60, No. 11, pp. 1379-1382, 2006.

40. Klein, J., et al., "Aluminum-Induced Crystallisation of Amorphous Silicon: Parameter Variation for Optimisation of the Process, *T3: Conference Record of the Thirty-First IEEE Photovoltaic Specialist Conference (IEEE Cat. No. 05CH37608)*, Piscataway, NJ, USA, pp. 1197-200, 2005.

41. Knaepen, W., et al., "In-Situ X-Ray Diffraction Study of Metal Induced Crystallization of Amorphous Silicon", *Thin Film Solids*, Vol. 516, p. 4946, 2007.

42. Cai, L., et al., "Large Grain Polycrystalline Silicon Film Produced by Nano-Aluminum-Enhanced Crystallization of Amorphous Silicon", *Electrochemical and Solid-State Letters*, Vol. 8, No. 7, pp. G179-G181, 2005.

43. Nair, R., and Zou, M., "Surface-Nano-Texturing by Aluminum-Induced Crystallization of Amorphous Silicon", *Surface & Coatings Technology*, Vol. 203, Nos. 5-7, pp. 675-9, 2008.

44. Zou, M., et al., "Self-Assembly of Si Nanoparticles Produced by Aluminum-Induced Crystallization of Amorphous Silicon Film", *Electrochemical and Solid-State Letters*, Vol. 10, No. 2, pp. K1-K9, 2007.

45. Wang, H., and Zou, M., "Amorphous Silicon Thickness Effect on Formation of Silicon Nanostructures by Aluminum-Induced Crystallization of Amorphous Silicon", *Electrochemical and Solid-State Letters*, Vol. 10, No. 8, pp. H224-H226, 2007.

46. Song, Y., et al., "Superhydrophobic Surfaces Prepared by Applying a Self-Assembled Monolayer to Silicon Micro/Nano-Textured Surfaces", *Nano Research*, Vol. 2, No. 2, pp. 143-150, 2009.

47. Kollias, K., and Wang, H., "Production of a Superhydrophilic Surface by Aluminum-Induced Crystallization of Amorphous Silicon", *Nanotechnology*, Vol. 19, pp. 465304-465310, 2008.

48. Beckford, S., and Zou, M., "Micro/Nano Engineering on Stainless Steel Substrates to Produce Superhydrophobic Surfaces", *Thin Film Solids*, 2011.

49. Morehead, J., and Zou, M., *Nano-Surface Engineering on Copper Substrate for Friction Reduction*, University of Arkansas, 2009.

50. Shirtcliffe, N., "Wetting and Wetting Transition on Copper-Based Super-Hydrophobic Surfaces", *Langmuir*, Vol. 21, No. 3, p. 938, **2005.**

51. Wu, W., et al., "Superhydrophobic Surface from Cu-Zn Alloy by One Step O_2 Concentration Dependent Etching", *Journal of Colloid and Interface Science*, Vol. 326, pp. 478-482, 2008.

52. Guo, Z., et al., "Fabrication of Superhydrophobic Copper by Wet Chemical Reaction", *Thin Solid Films*, Vol. 515, p. 7191, 2007.

53. Xu, W., et al., "Fabrication of Superhydrophobic Surfaces with Hierarchical Structure through a Solution-Immersion Process on Copper and Galvanized Iron Substrates", *Langmuir*, Vol. 24, No. 19, 2008.

54. Zhang, et al., "Fabrication of Superhydrophobic Copper Surface with Ultra-Low Water Roll Angle", *Applied Surface Science*, Vol. 256, pp. 1883-1887, 2010.

55. Wu, X., and Shi, G., "Fabrication of a Lotus-Like Micro-Nanoscale Binary Structured Surface and Wettability Modulation from Superhydrophilic to Superhydrophobic", *Nanotechnology*, Vol. 16, pp. 2056-2060, 2005.

56. Pan, Q., Jin, H., and Wang, H., "Fabrication of Superhydrophobic Surfaces on Interconnected $Cu(OH)_2$ Nanowires via Solution-Immersion", *Nanotechnology*, Vol. 18, No. 35, p. 355605, 2007.

57. Tang, K., et al., "Fabrication of Superhydrophilic Cu_2O and CuO Membranes", *Journal of Membrane Science*, Vol. 286, pp. 279-284, 2006.

58. Takata, Y., et al., "Pool Boiling on a Superhydrophilic Surface", *Journal of Energy Research*, Vol. 27, No. 2, pp. 111-119, 2003.

59. Qui, Y., and Liu, Z., "Nucleate Boiling on the Superhydrophilic Surface with a Small Water Impingement Jet", *Journal of Heat* Transfer, Vol. 51, Nos. 7-8, pp. 1683-1690, 2008.

60. Liu, et al., "Silicon Surface Structure-Controlled Oleophobicity", *Langmuir*, Vol. 26, No. 11, pp. 8909-8913, 2010.

61. Law, K., Zhao, H., and Sambhy, V., "Effects of Surface Texture and Chemistry on Surface Hydrophobicity and Oleophobicity", *NSTI-Nanotech 2009*, Vol. 3, pp. 177-179, 2009.

62. Ramos, S., et al., "Superoleophobic Behavior Induced by Nanofeatures on Oleophilic Surfaces", *Langmuir*, Vol. 26, No. 7, pp. 5141-5146, 2010.

63. Tsuji, I., Ohkubo, Y., and Ogawa, K., "Study on Super-Hydrophobic and Oleophobic Surfaces Prepared by Chemical Adsorption Technique", *Japanese Journal of Applied Physics*, Vol. 48, pp. 040205-1—040205-3, 2009.

64. Ohkubo, Y., et al., "Preparation and Characterization of Super-Hydrophobic and Oleophobic Surface", *Journal of Material Science*, Vol. 45, pp. 4963-4969, 2010.

65. Song, Y., Nair, R., and Zou, M., "Hydrophobic Surfaces Prepared by Aluminum-Induced Crystallization of Amorphous Silicon", *First International Conference on Integration and Commercialization of Micro and Nanosystems (MNC2007) Sanya, Hainan, China*, pp. 1537-1539, 2007.

66. Song, Y., et al., "Adhesion and Friction Properties of Micro/Nano-Engineered Superhydrophobic/Hydrophobic Surfaces", *Thin Film Solids*, Vol. 518, pp. 3801-3807, 2010.

67. Wang, H., Zou, M., and Wei, R., "Superhydrophilic Textured-Surfaces on Stainless Steel Substrates", *Thin Solid Films*, Vol. 518, No. 5, pp. 1571-1574, 2009.

68. Yoon, E. -S., et al., "An Experimental Study on the Adhesion at a Nano-Contact", Wear, Vol. 254, No 10, pp. 974-980, 2003.

69. Zou, M., Seale, W., and Wang, H., "Comparison of Tribological Performances of Nano- and Micro-Textured Surfaces", *Proceedings of the Institution of Mechanical Engineers, Part N, Journal of Nanoengineering and Nanosystems,*Vol. 219, No. 3, pp. 103-10, 2005.

70. Wang, H., *Mechanical and Tribological Study of Nickel Nanodot-Patterned Surfaces,* University of Arkansas, pp. 73-82, 2009.

71. Zou, M., and Nair, P., "Surface-Nano-Texturing by Aluminum-Induced Crystallization of Amorphous Silicon", *Surface Coatings and Technology*, Vol. 203, p. 675, 2008.

72. Zhang, D., Chow, T., and Wong, M., "A Polycrystalline Silicon Thin-Film Transistor with Self-Aligned Metal Electrodes formed using Aluminum-Induced Crystallization", *IEEE Transactions on Electron Devices, Special Issue on Silicon Carbide Devices and Technology*, Vol. 55, No. 8, pp. 2181-2186, 2008.

73. Website: http://www.copper.org/resources/properties/atomic/homepage.html, accessed date 8/28/2011.

74. Radnoczi, G., et al., "Al Induced Crystallization of a-Si", *Journal of Applied Physics*, Vol. 69, No. 9, pp. 6394-6399, 1991.

75. Bowden, F., and Tabor, D., *The Friction and Lubrication of Solids*, Clarendon Press, Oxford, 1950.

76. Suh, N., and Sin, H. -C., "The Genesis of Friction", *Wear*, Vol. 69, No. 1, pp. 91-114, 1981.

77. Komvopoulos, K., Saka, N., and Suh, N., "Mechanism of Friction in Boundary Lubrication", *Transactions ASME Journal of Tribology*, Vol. 107, No. 4, pp. 452-462, 1985.

78. Komvopoulos, K., Saka, N., and Suh, N., "Plowing Friction in Dry and Lubricated Metal Sliding", *Transactions ASME Journal of Tribology*, Vol. 108, No. 3, pp. 301-313, 1986.

79. Bernd, L., "Survey of Theory of Mechanical Face Seals", *Lubrication Engineering*, Vol. 24, No. 10, pp. 479-484, 1968.

80. Website: http//www.flowserve.com/files/files/literature/fsd/f2fv19n2eng.pdf, accessed date 8/28/2011.